



HAL
open science

CDC20B is required for deuterosome-mediated centriole production in 1 multiciliated cells

Diego R Revinski, Laure-Emmanuelle Zaragosi, Camille Boutin, Marie Deprez, Virginie Thomé, Olivier Rosnet, Anne-Sophie Gay, Agnès Paquet, Nicolas Pons, Gilles Ponzio, et al.

► To cite this version:

Diego R Revinski, Laure-Emmanuelle Zaragosi, Camille Boutin, Marie Deprez, Virginie Thomé, et al.. CDC20B is required for deuterosome-mediated centriole production in 1 multiciliated cells. *Nature Communications*, 2018, 9, pp.4668. 10.1038/s41467-018-06768-z . hal-02064869

HAL Id: hal-02064869

<https://hal.science/hal-02064869v1>

Submitted on 12 Mar 2019

HAL is a multi-disciplinary open access archive for the deposit and dissemination of scientific research documents, whether they are published or not. The documents may come from teaching and research institutions in France or abroad, or from public or private research centers.

L'archive ouverte pluridisciplinaire **HAL**, est destinée au dépôt et à la diffusion de documents scientifiques de niveau recherche, publiés ou non, émanant des établissements d'enseignement et de recherche français ou étrangers, des laboratoires publics ou privés.

1 **Title: CDC20B is required for deuterosome-mediated centriole production in**
2 **multiciliated cells**

3

4 **Authors:** Diego R. Revinski^{1†}, Laure-Emmanuelle Zaragosi^{2†}, Camille Boutin^{1†}, Sandra
5 Ruiz-Garcia², Marie Deprez², Virginie Thomé¹, Olivier Rosnet¹, Anne-Sophie Gay², Olivier
6 Mercey², Agnès Paquet², Nicolas Pons², Gilles Ponzio², Brice Marcet^{2*}, Laurent
7 Kodjabachian^{1*}, Pascal Barbry^{2*}

8

9 **Affiliations:**

10 ¹ Aix Marseille Univ, CNRS, IBDM, Marseille, France

11 ² Université Côte d'Azur, CNRS, IPMC, Sophia-Antipolis, France.

12 [†] These authors contributed equally

13 *Correspondence to: marcet@ipmc.cnrs.fr; laurent.kodjabachian@univ-amu.fr;
14 barbry@ipmc.cnrs.fr

15

16 **Keywords:** multiciliated cell, centriole, deuterosome, motile cilia, CDC20B, Separase, PLK1,
17 cell cycle, *Xenopus*, mouse, human

18

19

20 **Abstract:** Multiciliated cells (MCCs) harbour dozens to hundreds of motile cilia, which
21 generate hydrodynamic forces important in animal physiology. In vertebrates, MCC
22 differentiation involves massive centriole production by poorly characterized structures called
23 deuterosomes. Here, single-cell RNA sequencing reveals that human deuterosome-stage
24 MCCs are characterized by the expression of many cell cycle-related genes. We further
25 investigated the uncharacterized vertebrate-specific *cell division cycle 20B (CDC20B)* gene,
26 which hosts microRNA-449abc. We show that CDC20B protein associates to deuterosomes
27 and is required for centriole release and subsequent cilia production in mouse and *Xenopus*
28 MCCs. CDC20B interacts with PLK1, a kinase known to coordinate centriole disengagement
29 with the protease Separase in mitotic cells. Strikingly, over-expression of Separase rescues
30 centriole disengagement and cilia production in CDC20B-deficient MCCs. This work reveals
31 the shaping of a new biological function, deuterosome-mediated centriole production in
32 vertebrate MCCs, by adaptation of canonical and recently evolved cell cycle-related
33 molecules.

34

35 **Introduction**

36 Multiciliated cells (MCCs) are present throughout metazoan evolution and serve functions
37 ranging from locomotion of marine larvae and flatworms, to brain homeostasis, mucociliary
38 clearance of pathogens and transportation of oocytes in vertebrates¹⁻³. The formation of
39 MCCs requires the production of numerous motile cilia through a complex process called
40 multiciliogenesis^{2,3}. The transcriptional control of multiciliogenesis has been decrypted to a
41 large extent, through studies in *Xenopus* and mouse². Seating at the top of the cascade, the
42 Geminin-related factors GemC1⁴⁻⁷ and Multicilin^{8,9} (MCIDAS in mammals) are both
43 necessary and sufficient to initiate MCC differentiation. GemC1 and Multicilin in complex
44 with E2F transcription factors have been reported to activate the expression of Myb, FoxJ1,

45 Rfx2 and Rfx3, which collectively regulate the expression of a large body of effectors
46 required for the formation of multiple motile cilia^{4,5,8-11}. Recently, defective multiciliogenesis
47 caused by mutations in MCIDAS and Cyclin O (CCNO) has been associated with congenital
48 respiratory and fertility syndromes in human^{12,13}.

49 Each cilium sits atop a modified centriole, called a basal body (BB). After they exit from the
50 cell cycle, maturing MCCs face the challenge of producing dozens to hundreds of centrioles
51 in a limited time window. In vertebrate MCCs, bulk centriole biogenesis is mostly achieved
52 through an acentriolar structure named the deuterosome, although canonical amplification
53 from parental centrioles also occurs¹⁻³. The deuterosome was first described in early electron
54 microscopy studies of various multiciliated tissues including the mammalian lung¹⁴ and
55 oviduct^{15,16}, the avian trachea¹⁷, and the *Xenopus* tadpole epidermis and trachea¹⁸. In
56 mammalian MCCs, the deuterosome was described as a spherical mass of fibers organized
57 into an inner dense region and an outer, more delicate, corona¹⁶. In *Xenopus*, deuterosomes
58 were initially named procentriole organizers and were reported as dense amorphous masses¹⁸.

59 Recent studies have revealed that deuterosome-mediated centriole synthesis mobilizes key
60 components of the centriole-dependent duplication pathway of the cell cycle, including
61 CEP152, PLK4 and SAS6¹⁹⁻²¹. However, the deuterosome itself differs from the centriole and
62 may contain specific components. The identification of one such component, called DEUP1
63 for Deuterosome assembly protein 1, opened the possibility to investigate the deuterosome at
64 the molecular level²¹. In mouse tracheal ependymal cells, DEUP1 was detected in the core of
65 the deuterosome²¹. DEUP1, also known as CCDC67, is a conserved vertebrate paralogue of
66 CEP63, itself known for its importance in initiation of centriole duplication during the cell
67 cycle^{21,22}. Consistently, DEUP1 was shown to be essential for centriole multiplication in
68 mouse and *Xenopus* MCCs²¹. Both CEP63 and DEUP1 interact with CEP152, an essential
69 event for centriole duplication and multiplication in cycling cells and MCCs, respectively^{21,22}.

70 Once centriole multiplication is over, neo-synthesized centrioles must disengage from
71 deuterosomes and parental centrioles, convert into BBs and migrate apically to dock at the
72 plasma membrane to initiate cilium elongation.

73 In this study, we aimed at better understanding deuterosome biology. We found that the gene
74 *CDC20B* was specifically expressed in maturing MCCs during the phase of centriole
75 multiplication. We established the corresponding CDC20B protein as an essential regulator of
76 centriole-deuterosome disengagement. This work illustrates well the strong functional
77 relationships that exist between centriole release from deuterosomes and centriole
78 disengagement in mitotic cells. It also posits CDC20B as a new component of a “multiciliary
79 locus” that contains several gene products, either proteins, such as MCIDAS, CCNO or
80 CDC20B itself, or microRNAs, such as miR-449abc, which are all actively involved into
81 multiciliogenesis.

82

83 **Results**

84 **MCC single-cell transcriptome at deuterosome-stage**

85 To identify new regulators of centriole multiplication, we analyzed the transcriptome of
86 human airway epithelial cells (HAECs) at the differentiation stage corresponding to active
87 centriole multiplication²³ at the single-cell level (Fig. 1a). Gene expression data from 1663
88 cells was projected on a 2D space by *t*-distributed Stochastic Neighbor Embedding (tSNE)
89 (Fig. 1b). We identified a small group of 37 cells corresponding to maturing MCCs engaged
90 in deuterosome-mediated centriole amplification, as revealed by the specific expression of
91 *MCIDAS*⁸, *MYB*²⁴, and *DEUPI*²¹ (Fig. 1c,d and Supplementary Figure 1). This subpopulation
92 was characterized by the expression of known effectors of centriole synthesis, such as *PLK4*,
93 *STIL*, *CEP152*, *SASS6*, but also of cell cycle regulators, such as *CDK1*, *CCNB1*, *CDC20*,
94 *SGOL2* and *NEK2* (Fig. 1d, Supplementary Figure 1 and Supplementary Table 1). We

95 reasoned that uncharacterized cell cycle-related genes that are specific to this subpopulation
96 could encode new components of the deuterosome-dependent centriole amplification
97 pathway. A particularly interesting candidate in this category was *CDC20B* (Fig. 1d), which
98 is related to the cell cycle regulators *CDC20* and *FZR1*²⁵ (Supplementary Figure 2a). First, the
99 *CDC20B* gene is present in the vertebrate genomic locus that also contains the key MCC
100 regulators *MCIDAS*⁸ and *CCNO*¹³. Co-expression of *CDC20B*, *MCIDAS* and *CCNO*
101 throughout HAEC differentiation was indeed observed in an independent RNA sequencing
102 study, performed on a bulk population of HAECs (Supplementary Figure 2b). These results fit
103 well with the observation that the promoter of human *CDC20B* was strongly activated by the
104 *MCIDAS* partners E2F1 and E2F4 (Supplementary Figure 2c), as also shown in *Xenopus* by
105 others⁹ (Supplementary Figure 2d). Second, the *CDC20B* gene bears in its second intron the
106 miR-449 microRNAs, which were shown to contribute to MCC differentiation^{23, 26-30}. Finally,
107 in *Xenopus* epidermal MCCs, *cdc20b* transcripts were specifically detected during the phase
108 of centriole amplification (Supplementary Figure 2e-m). This first set of data pointed out the
109 specific and conserved expression pattern of *CDC20B* in immature MCCs. In the rest of this
110 study, we analyzed the putative role of *CDC20B* in deuterosome-mediated centriole
111 multiplication.

112

113 **Composition and organization of vertebrate deuterosomes**

114 We first conducted a series of immunofluorescence analyses to gain a better understanding of
115 deuterosome organization in mouse ependymal and *Xenopus* epidermal MCCs as models. In
116 whole-mounts of mouse ependymal walls, mature deuterosomes revealed by DEUP1 staining
117 appeared as circular structures around a lumen (Fig. 2a). We noticed that DEUP1 also stained
118 fibers emanating from the core into the corona. Nascent centrioles revealed by the marker
119 FOP were organized around the DEUP1-positive core ring. STED super-resolution

120 microscopy helped to better appreciate the regular organization of individual FOP-positive
121 procentrioles (Fig. 2b). Proximity labeling assays have revealed that when ectopically
122 expressed in centrosomes CCDC67/DEUP1 is found close to Pericentrin (PCNT) and γ -
123 tubulin, two main components of the pericentriolar material (PCM)³¹. Interestingly, we found
124 that PCNT was present in the deuterosome corona (Fig. 2a), and STED microscopy further
125 revealed that PCNT formed fibers around growing procentrioles (Fig. 2b). γ -tubulin staining
126 was detected in the DEUP1-positive deuterosome core, as well as in the corona (Fig. 2a).
127 STED microscopy indicated that PCNT and γ -tubulin stained distinct interwoven fibers in the
128 deuterosome corona. Next, we stained immature *Xenopus* epidermal MCCs with γ -Tubulin
129 and Centrin to reveal centriole amplification platforms. These platforms displayed irregular
130 shapes and sizes (Fig. 2c), in agreement with early electron microscopy studies¹⁸. Expression
131 of low amounts of GFP-Deup1 in MCCs induced by Multicilin confirmed that active
132 deuterosomes are embedded in γ -Tubulin-positive masses (Fig. 2d). Overall, this analysis is
133 consistent with early ultrastructural studies, as the deuterosome core and corona can be
134 distinguished by the presence of DEUP1 and PCNT, respectively. Moreover, γ -tubulin is a
135 conserved marker of centriole amplification platforms in vertebrate MCCs. By analogy to the
136 organization of the centrosome, we propose to coin the term perideuterosomal material
137 (PDM) to describe the corona, as this region may prove important for deuterosome function.

138

139 **CDC20B associates to vertebrate deuterosomes**

140 We then analyzed the subcellular localization of CDC20B protein in deuterosome-stage
141 mouse and *Xenopus* MCCs. In immature mouse tracheal MCCs, double immunofluorescence
142 revealed the association of CDC20B to DEUP1-positive deuterosomes (Fig. 3a). We noticed
143 that CDC20B tended to associate primarily to large DEUP1 foci. As deuterosomes grow as
144 they mature²¹, this suggests that CDC20B may penetrate into the deuterosomal environment

145 at a late stage of the centriole multiplication process. The same observation was made when
146 comparing CDC20B staining in the region of immature and mature deuterosomes of mouse
147 ependymal MCCs (Fig. 3b). As double DEUP1/CDC20B staining could not be performed on
148 these cells, we analyzed CDC20B distribution relative to FOP-positive procentrioles. In early
149 deuterosome-stage MCCs, CDC20B was expressed at low levels and FOP staining was
150 mostly concentrated in a large amorphous cloud (Fig. 3b). In such cells, no CDC20B staining
151 was detected in association to FOP-positive procentrioles growing around deuterosomes. In
152 contrast, in mature deuterosome-stage MCCs, CDC20B was enriched in the innermost part of
153 the PDM, probably very close to the deuterosome core (Fig. 3b). Further evidence was
154 provided with a custom-made polyclonal antibody (Supplementary Figure 3b,c) used to
155 analyze Cdc20b protein distribution in *Xenopus* epidermal MCCs. Here also, Cdc20b was
156 found associated to Deup1-positive deuterosomes actively engaged in centriole synthesis (Fig.
157 3c). We finally analyzed the distribution of CDC20B in mature MCCs. As previously
158 reported, the CDC20B protein was detected near BBs²³, but also in cilia of fully differentiated
159 human airway MCCs (Supplementary Figure 4a-c). This was confirmed by proximity ligation
160 assays that revealed a tight association of CDC20B with Centrin2 and acetylated α -Tubulin,
161 in BBs and cilia, respectively (Supplementary Figure 4d-f). Fluorescent immunostaining also
162 revealed the presence of Cdc20b in the vicinity of BBs in *Xenopus* epidermal MCCs
163 (Supplementary Figure 4g-i). In contrast, no cilia staining was observed in these cells.
164 Altogether, our analyses revealed that in three distinct types of MCCs in two distant
165 vertebrate species, CDC20B is tightly associated to mature deuterosomes. We next
166 investigated whether it may control their function.

167

168 **CDC20B is required for multiciliogenesis in vertebrates**

169 For that purpose, *Cdc20b* was knocked down in mouse ependymal MCCs, through post-natal
170 brain electroporation of three distinct shRNAs. One of them, sh274, which targets the
171 junction between exons 3 and 4, and can therefore only interact with mature mRNA, was
172 useful to rule out possible interference with the production of miR-449 molecules from the
173 *Cdc20b* pre-mRNA (Supplementary Figure 5a). Five days after electroporation, all three
174 shRNAs significantly reduced the expression of CDC20B in deuterosome-stage MCCs (Fig.
175 4c), but did not alter MCC identity as revealed by FOXJ1 expression (Fig. 4a,b,d). Centriole
176 production by deuterosomes was analyzed by FOP/DEUP1 double staining nine days after
177 electroporation. At this stage, control MCCs had nearly all released their centrioles and
178 disassembled their deuterosomes (Fig. 4e,g). In sharp contrast, *Cdc20b* shRNAs caused a
179 significant increase in the number of defective MCCs that displayed centrioles still engaged
180 on deuterosomes (Fig. 4f,g). Fifteen days after electroporation, a majority of CDC20B-
181 deficient MCCs still showed a severely reduced number of released centrioles, and
182 consequently lacked cilia (Fig. 4h-k).

183 *Cdc20b* was also knocked down in *Xenopus* epidermal MCCs, through injection of two
184 independent morpholino antisense oligonucleotides targeting either the ATG (Mo ATG), or
185 the exon 1/intron 1 junction (Mo Spl) (Supplementary Figure 5b). The efficiency of Mo ATG
186 was verified through fluorescence extinction of co-injected *Cdc20b*-Venus (Supplementary
187 Figure 5c). RT-PCR confirmed that Mo Spl caused intron 1 retention (Supplementary Figure
188 5d), which was expected to introduce a premature stop codon, and to produce a *Cdc20b*
189 protein lacking 96% of its amino-acids, likely to undergo unfolded protein response-mediated
190 degradation. Thus, both morpholinos were expected to generate severe loss of *Cdc20b*
191 function. Consistent with this interpretation, both morpholinos strongly reduced *Cdc20b*
192 immunostaining in deuterosome-stage MCCs (Supplementary Figure 5e). We verified that
193 neither morpholinos caused *p53* transcript up-regulation (Supplementary Figure 5f), a non-

194 specific response to morpholinos that is sometimes detected in zebrafish embryos³².
195 Importantly, whole-mount *in situ* hybridization indicated that miR-449 expression was not
196 perturbed in the presence of either morpholino (Supplementary Figure 5g). We found that
197 *cdc20b* knockdown did not interfere with acquisition of the MCC fate (Supplementary Figure
198 6a-e), but severely impaired multiciliogenesis, as revealed by immunofluorescence and
199 electron microscopy (Fig. 5a-i). This defect stemmed from a dramatic reduction in the number
200 of centrioles, and poor docking at the plasma membrane (Fig. 5g-o and Supplementary Figure
201 6f-k). Importantly, centrioles and cilia were rescued in Mo Spl MCCs by co-injection of
202 *cdc20b*, *venus-cdc20b* or *cdc20b-venus* mRNAs (Fig. 5j-o and Supplementary Figure 6f-k). In
203 normal condition, *Xenopus* epidermal MCCs arise in the inner mesenchymal layer and
204 intercalate into the outer epithelial layer, while the process of centriole amplification is
205 underway³³. To rule out secondary defects due to poor radial intercalation, we assessed the
206 consequences of *cdc20b* knockdown in MCCs induced in the outer layer by Multicilin
207 overexpression⁸. Like in natural MCCs, Cdc20b proved to be essential for the production of
208 centrioles and cilia in response to Multicilin activity (Supplementary Figure 7a-g). We also
209 noted that the apical actin network that normally surrounds BBs was **disrupted** in absence of
210 Cdc20b, although this defect could be secondary to the absence of centrioles (Supplementary
211 Figure 7d-g). Centrioles in Cdc20b morphant cells often formed clusters, suggesting that
212 disengagement from deuterosomes could have failed (Fig. 5l,m). To better assess this process,
213 we injected GFP-Deup1 in Multicilin-induced MCCs and stained centrioles with Centrin. In
214 mature control MCCs, deuterosomes were disassembled, centrioles were converted into BBs,
215 had docked and initiated cilium growth (Fig. 5p,s). In contrast, both morpholinos caused a
216 dramatic increase in the number of defective MCCs, which were devoid of cilia and displayed
217 centrioles still engaged on deuterosomes (Fig. 5q-u). Altogether our functional assays in
218 mouse and *Xenopus* indicate that CDC20B is required for centriole disengagement from

219 deuterosomes and subsequent ciliogenesis in MCCs. We next investigated the molecular
220 mechanism of action of CDC20B underlying its role in centriole release.

221

222 **Partners and effectors of CDC20B reveal its mechanism of action**

223 In mitotic cells, centriole disengagement is necessary to license centriole duplication in the
224 following cell cycle³⁴. This process is known to depend on the coordinated activities of the
225 mitotic kinase PLK1 and the protease Separase³⁵. One proposed mechanism involves the
226 phosphorylation of PCNT by PLK1, which induces its cleavage by Separase, thereby
227 allowing centriole disengagement through disassembly of the PCM^{36,37}. Separase is known to
228 be activated by the degradation of its inhibitor Securin, which is triggered by the Anaphase
229 Promoting Complex (APC/C) upon binding to CDC20²⁵. *PLK1*, *Separase (ESPL1)*, *Securin*
230 (*PTTG1*), *CDC20* and *PCNT* were all found to be expressed in human deuterosome-stage
231 MCCs (Fig. 1d and Supplementary Figure 1). We have shown above that PCNT is present in
232 the PDM and a recent study revealed the presence of CDC20 and the APC/C component
233 APC3 in mouse ependymal MCCs at the stage of centriole disengagement³⁸. Based on this
234 large body of information, we hypothesized that centriole-deuterosome disengagement
235 involves the coordinated activities of PLK1 and Separase, and that CDC20B would be
236 involved in this scenario. *CDC20B* encodes a protein of about 519 amino-acids largely
237 distributed across the vertebrate phylum²³. In its C-terminal half, CDC20B contains seven
238 well conserved WD40 repeats, predicted to form a β -propeller, showing 49% and 37%
239 identity to CDC20 and FZR1 repeats, respectively (Supplementary Figure 2a). However,
240 CDC20B lacks canonical APC/C binding domains (Supplementary Figure 2a). Using mass
241 spectrometry on immunoprecipitated protein complexes from transfected HEK cells, we could
242 identify multiple APC/C components interacting with CDC20 but not with CDC20B
243 (Supplementary Table 2). We conclude that CDC20B is probably incapable of activating

244 APC/C. Interestingly, an unbiased interactome study reported association of CDC20B with
245 PLK1³⁹. Using reciprocal co-immunoprecipitation assays in HEK transfected cells, we
246 confirmed that CDC20B and PLK1 could be found in the same complex (Fig. 6a and
247 Supplementary Figure 8). This suggested that CDC20B could cooperate with PLK1 to trigger
248 centriole disengagement. Consistent with this hypothesis, we found that PLK1 was enriched
249 in the PDM of mature deuterosomes in mouse ependymal MCCs (Fig. 6b), in agreement with
250 a recent report³⁸. Another interesting partner of CDC20B identified in a second unbiased
251 interactome study⁴⁰ was SPAG5 (Astrin), which was reported to control timely activation of
252 Separase during the cell cycle^{41, 42}. Using the same strategy as above, we could detect
253 CDC20B and SPAG5 in the same complex (Fig. 6c and Supplementary Figure 8). As SPAG5
254 was found associated to DEUP1 in a proximity labeling assay³¹, we assessed its localization
255 in deuterosomes. Strikingly, SPAG5 was detectable in mature deuterosomes of mouse
256 ependymal MCCs, with a clear enrichment in the deuterosome core (Fig. 6d). Finally,
257 reciprocal co-immunoprecipitations revealed that CDC20B and DEUP1 were detected in the
258 same complex when co-expressed in HEK cells (Fig. 6e and Supplementary Figure 8).
259 Consistent with this result, we observed that RFP-Cdc20b was recruited around spherical
260 Deup1-GFP structures positive for γ -Tubulin and Centrin in *Xenopus* epidermal MCCs
261 (Supplementary Figure 7h-m). This series of experiments suggested that CDC20B could
262 participate in the assembly of a protein complex in mature deuterosomes, required to
263 coordinate the activities of PLK1 and Separase for centriole disengagement. As Separase is
264 the last effector in this scenario, we tested whether over-expressing human Separase in
265 *Xenopus cdc20b* morphant MCCs could rescue centriole disengagement. In support to our
266 hypothesis, over-expression of wild-type, but not protease-dead Separase, efficiently rescued
267 centriole disengagement and cilia formation in *cdc20b* morphant MCCs (Fig. 7a-g and
268 Supplementary Figure 7n-s). Separase could also rescue multiciliogenesis in Multicilin-

269 induced MCCs injected with *cdc20b* Mos (Supplementary Figure 7t-z). We conclude that
270 CDC20B is involved in Separase-mediated release of mature centrioles from deuterosomes in
271 vertebrate MCCs (Fig. 7h).

272

273 **Discussion**

274 In this study, we report for the first time the essential and conserved role of CDC20B in
275 vertebrate multiciliogenesis. Our data suggest that the presence of CDC20B in the
276 perideuterosomal region is necessary to allow centriole disengagement. We note, however,
277 that our data, which are based on partial knockdowns, remain compatible with an earlier
278 function of CDC20B in promoting deuterosome assembly and/or activity. A total genetic
279 knockout of *Cdc20b* should help to assess this possibility in mouse tracheal and ependymal
280 MCCs. By analogy to mitosis, we propose that CDC20B is involved in Separase-dependent
281 proteolysis at deuterosomes, allowing the release of mature centrioles and subsequent
282 ciliogenesis. This view is consistent with a recent report showing that centriole
283 disengagement in murine ependymal MCCs involves the activities of PLK1, a partner of
284 CDC20B, and APC/C, the activator of Separase³⁸. The central question arising from our work
285 then becomes: how are CDC20B and Separase activities integrated? The simple scenario of a
286 CDC20-like function of CDC20B is very unlikely as it does not appear to bind APC/C
287 (Supplementary Table 2). CDC20 was detected in cultured murine ependymal MCCs during
288 the phase of centriole disengagement³⁸, and FZR1 genetic ablation was reported to cause
289 reduced production of centrioles and cilia in the same cells⁴³. APC/C is therefore likely
290 activated in maturing MCCs by its classical activators, CDC20 and/or FZR1, leading to
291 Separase activation through degradation of its inhibitor Securin. In that context, we propose
292 that additional factors linked directly or indirectly to CDC20B may contribute to activation of
293 Separase. It was shown that SPAG5 inhibits or activates Separase depending on its status of

294 phosphorylation^{41, 42}. As the phosphorylation status of SPAG5 was shown to be controlled by
295 PLK1⁴⁴, our data suggest that the CDC20B/PLK1/SPAG5 complex could control the timing
296 of Separase activation locally in deuterosomes. It is therefore possible that multiple modes of
297 activation of Separase may act in parallel to trigger the release of neo-synthesized centrioles
298 in maturing MCCs. Alternatively, different pathways may be used in distinct species, or in
299 distinct types of MCCs. An important question for future studies regards the identity of PLK1
300 and Separase substrates involved in centriole disengagement. Work on mitotic cells^{36, 37} and
301 our own analysis suggest that PCNT may represent a prime target. Another potentially
302 relevant candidate could be DEUP1 itself as it is clear that deuterosomes are disassembled
303 after the release of centrioles. In that respect, it is interesting to note the presence of multiple
304 PLK1 consensus phosphorylation sites in human, mouse and *Xenopus* DEUP1.

305 In this study, we have introduced the notion of perideuterosomal material, in analogy to the
306 pericentriolar material. It is striking that the two main components of the PCM, PCNT and γ -
307 Tubulin, are also present in the PDM, which begs the question whether additional PCM
308 proteins may be present in the PDM. The PDM may constitute a platform to sustain
309 procentriole growth, through the concentration and delivery of elementary parts. It could also
310 play a mechanical role to hold in place the growing procentrioles. Future work should
311 evaluate deuterosome-mediated centriole synthesis in absence of major PDM components.

312 We found that beyond its association to deuterosomes during the phase of centriole
313 amplification, CDC20B was also associated to BBs and cilia in fully differentiated
314 mammalian MCCs. This dual localization is consistent with failed ciliogenesis upon CDC20B
315 knockdown in mouse ependymal MCCs. However, while we could detect Cdc20b near BBs
316 of mature MCCs in *Xenopus*, we found no evidence of its presence in cilia. Furthermore, cilia
317 were rescued by Separase overexpression in Cdc20b morphant MCCs. This suggests that
318 Cdc20b is not required for ciliogenesis in this species, although it could potentially contribute

319 to cilium structure and/or function. Thus, refined temporal and spatial control of *CDC20B*
320 inhibition will be needed to study its function beyond centriole synthesis.

321 This and previous studies^{23, 26-28} establish that the miR-449 cluster and its host gene *CDC20B*
322 are commonly involved in multiciliogenesis. Consistent with its early expression, it was
323 suggested that miR-449 controls cell cycle exit and entry into differentiation of MCCs^{23, 27, 30}.
324 This study reveals that *CDC20B* itself is involved in the production of centrioles, the first key
325 step of the multiciliogenesis process. From that perspective, the nested organization of miR-
326 449 and *CDC20B* in vertebrate genomes, which allows their coordinated expression, appears
327 crucial for successful multiciliogenesis.

328 It is also noteworthy to point out the location of this gene in a genomic locus where
329 congenital mutations in *MCIDAS* and *CCNO* were recently shown to cause a newly-
330 recognized MCC-specific disease, called Reduced Generation of Multiple motile Cilia
331 (RGMC). RGMC is characterized by severe chronic lung infections and increased risk of
332 infertility^{12, 13}. Its location in the same genetic locus as *MCIDAS* and *CCNO* makes *CDC20B*
333 a putative candidate for RGMC. By extension, new deuterosome-stage specific genes
334 uncovered by scRNA-seq in this study also represent potential candidates for additional
335 RGMC mutations.

336 Previous works have established the involvement of the centriole duplication machinery
337 active in S-phase of the cell cycle, during centriole multiplication of vertebrate post-mitotic
338 MCCs¹⁹⁻²¹. Our study further reveals a striking analogy between centriole disengagement
339 from deuterosomes in MCCs, and centriole disengagement that occurs during the M/G1
340 transition of the cell cycle (Fig. 7g). Thus, it appears that centriole production in MCCs
341 recapitulates the key steps of the centriole duplication cycle³⁴. However, the cell cycle
342 machinery must adapt to the acentriolar deuterosome to massively produce centrioles. Such
343 adaptation appears to involve physical and functional interactions between canonical cell

344 cycle molecules, such as CEP152 and PLK1, and recently evolved cell cycle-related
345 deuterosomal molecules, such as DEUP1²¹ and CDC20B. It remains to examine whether
346 additional deuterosomal cell cycle-related molecules have emerged in the vertebrate phylum
347 to sustain massive centriole production.

348 In conclusion, this work illustrates how coordination between ancestral and recently evolved
349 cell cycle-related molecules can give rise to a new differentiation mechanism in vertebrates.

350

351 **Methods**

352 Subjects/human samples

353 Inferior turbinates were from patients who underwent surgical intervention for nasal
354 obstruction or septoplasty (provided by L. Castillo, Nice University Hospital, France). The
355 use of human tissues was authorized by the bioethical law 94-654 of the French Public Health
356 Code and written consent from the patients.

357

358 Single-cell RNA sequencing of Human Airway Epithelial Cells (HAECs)

359 HAECs cultures were derived from nasal mucosa of inferior turbinates. After excision, nasal
360 inferior turbinates were immediately immersed in Ca²⁺/Mg²⁺-free HBSS supplemented with
361 25 mM HEPES, 200 U/mL penicillin, 200 µg/mL streptomycin, 50 µg/mL gentamicin sulfate,
362 and 2.5 µg/ml amphotericin B (all reagents from Gibco). After repeated washes with cold
363 supplemented HBSS, tissues were digested with 0.1% Protease XIV from *Streptomyces*
364 *Griseus* (Sigma) overnight at 4°C. After incubation, fetal calf serum (FCS) was added to a
365 final concentration of 10%, and nasal epithelial cells were detached from the stroma by gentle
366 agitation. Cell suspensions were further dissociated by trituration through a 21G-needle and
367 then centrifuged at 150g for 5 min. The pellet was resuspended in supplemented HBSS
368 containing 10% FCS and centrifuged again. The second cell pellet was then suspended in

369 Dulbecco's Modified Eagle's Medium (DMEM, Gibco) containing 10% FCS and cells were
370 plated (20 000 cells per cm²) on 75 cm²-flasks coated with rat-tail collagen I (Sigma-Aldrich).
371 Cells were incubated in a humidified atmosphere of 5% CO₂ at 37°C. Culture medium was
372 replaced with Bronchial Epithelium Basal Medium (BEBM, Lonza) supplemented with
373 BEGM SingleQuot Kit Supplements (Lonza) on the day after and was then changed every
374 other day. After 4 to 5 days of culture, after reaching about 70% confluence, cells were
375 detached with trypsin-EDTA 0.05% (Gibco) for 5 min and seeded on Transwell® permeable
376 supports (6.5 mm diameter; 0.4 µm pore size; Corning), in BEGM medium, with a density of
377 30 000 cells per Transwell®. Once the cells have reached confluence (typically after 5 days),
378 they were induced to differentiate at the air-liquid interface by removing medium at the apical
379 side of the Transwell®, and by replacing medium at the basal side with DMEM:BEBM (1:1)
380 supplemented with BEGM SingleQuot Kit Supplements. Culture medium was changed every
381 other day. Single-cell analysis was performed after 14 days of culture at the air-liquid
382 interface, which corresponds to the maximum centriole multiplication stage. To obtain a
383 single-cell suspension, cells were incubated with 0.1% protease type XIV from *Streptomyces*
384 *griseus* in supplemented HBSS for 4 hours at 4°C degrees. Cells were gently detached from
385 Transwells® by pipetting and then transferred to a microtube. 50 units of DNase I (EN0523
386 Thermo Fisher Scientific) per 250 µL were directly added and cells were further incubated at
387 room temperature for 10 min. Cells were centrifuged (150g for 5 min) and resuspended in 500
388 µL supplemented HBSS containing 10% FCS, centrifuged again (150g for 5 min) and
389 resuspended in 500 µL HBSS before being mechanically dissociated through a 26G syringe (4
390 times). Finally, cell suspensions were filtered through a Scienceware® Flowmi™ Cell
391 Strainer (40µm porosity), centrifuged (150g for 5 min) and resuspended in 500 µL of cold
392 HBSS. Cell concentration measurements were performed with Scepter™ 2.0 Cell Counter
393 (Millipore) and Countess™ automated cell counter (ThermoFisher Scientific). Cell viability

394 was checked with Countess™ automated cell counter (ThermoFisher Scientific). All steps
395 except the DNase I incubation were performed on ice. For the cell capture by the 10X
396 genomics device, the cell concentration was adjusted to 300 cells/μl in HBSS aiming to
397 capture 1500 cells. We then followed the manufacturer's protocol (Chromium™ Single Cell
398 3' Reagent Kit, v2 Chemistry) to obtain single cell 3' libraries for Illumina sequencing.
399 Libraries were sequenced with a NextSeq 500/550 High Output v2 kit (75 cycles) that allows
400 up to 91 cycles of paired-end sequencing: the forward read had a length of 26 bases that
401 included the cell barcode and the UMI; the reverse read had a length of 57 bases that
402 contained the cDNA insert. CellRanger Single-Cell Software Suite v1.3 was used to perform
403 sample demultiplexing, barcode processing and single-cell 3' gene counting using standards
404 default parameters and human build hg19. Additional analyses were performed using R.
405 Pseudotemporal ordering of single cells was performed with the last release of the Monocle
406 package⁴⁵. Cell cycle scores were calculated by summing the normalized intensities of genes
407 belonging to phase-specific gene sets then centered and scaled by phase. Gene sets for each
408 phase were curated from previously described sets of genes⁴⁶ (Table S2). Data was submitted
409 to the GEO portal under series reference GSE103518. Data shown in Figure 1 is
410 representative of 4 independent experiments performed on distinct primary cultures.

411

412 RNA sequencing of HAECs

413 For Figure S3A, three independent HAEC cultures (HAEC1, HAEC2, HAEC3) were
414 triggered to differentiate in air-liquid interface (ALI) cultures for 2 days (ALI day 2,
415 undifferentiated), ALI day 14 (first cilia) or ALI day 28 (well ciliated). RNA was extracted
416 with the miRNeasy mini kit (Qiagen) following manufacturer's instructions. mRNA-seq was
417 performed from 2 μg of RNA that was first subjected to mRNA selection with Dynabeads®
418 mRNA Purification Kit (Invitrogen). mRNA was fragmented 10 min at 95°C in RNaseIII

419 buffer (Invitrogen) then adapter-ligated, reverse transcribed and amplified (6 cycles) with the
420 reagents from the NEBNext Small RNA Library Prep Set for SOLiD. Small RNA-seq was
421 performed from 500 ng RNA with the NEBNext Small RNA Library Prep Set for SOLiD (12
422 PCR cycles) according to manufacturer's instructions. Both types of amplified libraries were
423 purified on Purelink PCR micro kit (Invitrogen), then subjected to additional PCR rounds (8
424 cycles for RNA-seq and 4 cycles for small RNA-seq) with primers from the 5500 W
425 Conversion Primers Kit (Life Technologies). After Agencourt® AMPure® XP beads
426 purification (Beckman Coulter), libraries were size-selected from 150 nt to 250 nt (for RNA-
427 seq) and 105 nt to 130 nt (for small RNA-seq) with the LabChip XT DNA 300 Assay Kit
428 (Caliper Lifesciences), and finally quantified with the Bioanalyzer High Sensitivity DNA Kit
429 (Agilent). Libraries were sequenced on SOLiD 5500XL (Life Technologies) with single-end
430 50b reads. SOLiD data were analyzed with lifescape v2.5.1, using the small RNA pipeline for
431 miRNA libraries and whole transcriptome pipeline for RNA-seq libraries with default
432 parameters. Annotation files used for production of raw count tables correspond to Refseq
433 Gene model v20130707 for mRNAs and miRBase v18 for small RNAs. Data generated from
434 RNA sequencing were then analyzed with Bioconductor (<http://www.bioconductor.org>)
435 package DESeq and size-factor normalization was applied to the count tables. Heatmaps were
436 generated with GenePattern using the "Hierarchical Clustering" Module, applying median
437 row centering and Euclidian distance.

438

439 Re-analysis of *Xenopus* E2F4 Chip-seq and RNA-seq

440 RNA-seq (samples GSM1434783 to GSM1434788) and Chip-seq (samples GSM1434789 to
441 GSM1434792) data were downloaded from GSE59309. Reads from RNA-seq were aligned to
442 the *Xenopus laevis* genome release 7.1 using TopHat2⁴⁷ with default parameters.
443 Quantification of genes was then performed using HTSeq-count⁴⁸ release 0.6.1 with "-m

444 intersection-nonempty” option. Normalization and statistical analysis were performed using
445 Bioconductor package DESeq2⁴⁹. Differential expression analysis was done between
446 Multicilin-hGR alone versus Multicilin-hGR in the presence of E2f4ΔCT. Reads from ChIP-
447 seq were mapped to the *Xenopus laevis* genome release 7.1 using Bowtie2⁵⁰. Peaks were
448 called and annotated according to their positions on known exons with HOMER⁵¹. Peak
449 enrichments of E2F4 binding site in the promoters of centriole genes and cell cycle genes⁹
450 were estimated in presence or absence of Multicilin and a ratio of E2F4 binding (Multicilin vs
451 no Multicilin) was calculated.

452

453 Promoter reporter studies

454 The human *CDC20B* promoter was cloned into the pGL3 Firefly Luciferase reporter vector
455 (Promega) with SacI and NheI cloning sites. The promoter sequenced ranged from -1073 to
456 +104 relative to the transcription start site. 37.5 ng of pGL3 plasmid were applied per well.
457 pCMV6-Neg, pCMV6-E2F1 (NM_005225) and pCMV6-E2F4 (NM_001950) constructs
458 were from Origene. 37.5 ng of each plasmid was applied per well. 25 ng per well of pRL-
459 CMV (Promega) was applied in the transfection mix for transfection normalization (Renilla
460 luciferase). HEK 293T cells were seeded at 20 000 cells per well on 96-well plates. The
461 following day, cells were transfected with the indicated plasmids (100 ng of total DNA) with
462 lipofectamine 3000 (Invitrogen). After 24 hours, cells were processed with the DualGlo kit
463 (Promega) and luciferase activity was recorded on a plate reader.

464

465 Proximity ligation Assays

466 Fully differentiated HAECs were dissociated by incubation with 0.1% protease type XIV
467 from *Streptomyces griseus* (Sigma-Aldrich) in HBSS (Hanks' balanced salts) for 4 hours at
468 4°C. Cells were gently detached from the Transwells® by pipetting and then transferred to a

469 microtube. Cells were then cytocentrifuged at 300 rpm for 8 min onto SuperFrostPlus slides
470 using a Shandon Cytospin 3 cytocentrifuge. Slides were fixed for 10 min in methanol at -
471 20°C for Centrin2 and ZO1 assays, and for 10 min in 4% paraformaldehyde at room
472 temperature and then permeabilized with 0.5% Triton X-100 in PBS for 10 min for
473 Acetylated- α -tubulin assays. Cells were blocked with 3% BSA in PBS for 30 min. The
474 incubation with primary antibodies was carried out at room temperature for 2 h. Then, mouse
475 and rabbit secondary antibodies from the Duolink® Red kit (Sigma-Aldrich) were applied and
476 slides were processed according to manufacturer's instructions. Images were acquired using
477 the Olympus Fv10i confocal imaging systems with 60X oil immersion objective and Alexa
478 647 detection parameters.

479

480 Animals

481 All experiments were performed following the Directive 2010/63/EU of the European
482 parliament and of the council of 22 September 2010 on the protection of animals used for
483 scientific purposes. Experiments on *Xenopus laevis* and mouse were approved by the
484 'Direction départementale de la Protection des Populations, Pôle Alimentation, Santé
485 Animale, Environnement, des Bouches du Rhône' (agreement number F 13 055 21). Mouse
486 experiments were approved by the French ethical committee n°14 (permission number: 62-
487 12112012). Timed pregnant CD1 mice were used (Charles Rivers, Lyon, France).

488

489 Immunostaining on mouse ependyma

490 Dissected brains were subjected to 12 min fixation in 4% paraformaldehyde, 0.1% Triton X-
491 100, blocked 1 hour in PBS, 3% BSA, incubated overnight with primary antibodies diluted in
492 PBS, 3% BSA, and incubated 1 h with secondary antibodies at room temperature. Ependyma
493 were dissected further and mounted with Mowiol before imaging using an SP8 confocal

494 microscope (Leica microsystems) equipped with a 63x oil objective. The same protocol was
495 used to prepare samples for super-resolution acquisition. Pictures were acquired with a TCS
496 SP8 STED 3X microscope equipped with an HC PL APO 93X/1.30 GLYC motCORR™
497 objective (Leica microsystems). Pericentrin was revealed using Alexa 514 (detection 535-
498 564nm, depletion 660nm), γ -tubulin was revealed using Alexa 568 (detection 582-667nm,
499 depletion 775), and FOP was revealed using Alexa 488 (detection 498-531nm, depletion
500 592nm). Pictures were deconvoluted using Huygens software. Maximum intensity projection
501 of 3 deconvoluted pictures is presented in Figure 4G. Primary antibodies: rabbit anti-CDC20B
502 (1:500; Proteintech, 133376-1-AP), mouse IgG anti-PLK1 (1:500; Thermo Fisher, 33-1700),
503 rabbit anti-Pericentrin (1:500, Abcam, ab4448), mouse IgG1 anti-FoxJ1 (1:1000; eBioscience,
504 14-9965), rabbit anti-Deup1 (1:1000; kindly provided by Dr Xueliang Zhu), rabbit anti-Deup1
505 (1:250; Proteintech, 24579-1-AP), mIgG1 anti- γ -Tubulin (clone GTU88) (1:250; Abcam, Ab
506 11316), rabbit anti-ZO1 (1:600; Thermo Fisher Scientific, 61-7300), rabbit anti-Spag5 (1:500;
507 Proteintech, 14726-1-AP), mouse IgG1 anti-ZO1 (1:600; Invitrogen, 33-9100), mouse IgG2b
508 anti-FGFR1OP (FOP) (1:2000; Abnova, H00011116-M01), mouse IgG1 anti- α -tubulin
509 (1:500; Sigma-Aldrich, T9026). Secondary antibodies: Alexa Fluor 488 goat anti-rabbit
510 (1:800; Thermo Fisher Scientific, A-11034), Alexa Fluor 647 goat anti-rabbit (1:800; Thermo
511 Fisher Scientific, A-21244), Alexa Fluor 514 goat anti-rabbit (1:800; Thermo Fisher
512 Scientific, A-31558), Alexa Fluor 488 goat anti-mouse IgG2b (1:800; Thermo Fisher
513 Scientific, A-21141), Alexa Fluor 568 goat anti-mouse IgG2b (1:800; Thermo Fisher
514 Scientific, A-21144), Alexa Fluor 488 goat anti-mouse IgG2a (1:800; Thermo Fisher
515 Scientific, A-21131), Alexa Fluor 568 goat anti-mouse IgG1 (1:800; Thermo Fisher
516 Scientific, A-21134), Alexa Fluor 647 goat anti-mouse IgG1 (1:800; Thermo Fisher
517 Scientific, A-21240).

518

519 Mouse constructs

520 Expression constructs containing shRNA targeting specific sequences in the CDC20B coding
521 sequence under the control of the U6 promoter were obtained from Sigma-Aldrich (ref.
522 TRCN0000088273 (sh273), TRCN0000088274 (sh274), TRCN0000088277 (sh277)). PCX-
523 mcs2-GFP vector (Control GFP) kindly provided by Xavier Morin (ENS, Paris, France), and
524 U6 vector containing a validated shRNA targeting a specific sequence in the NeuroD1 coding
525 sequence⁵² (Control sh, ref. TRCN0000081777, Sigma-Aldrich) were used as controls for
526 electroporation experiments.

527

528 Postnatal mouse brain electroporation

529 The detailed protocol for postnatal mouse brain electroporation established by Boutin and
530 colleagues⁵³ was used with minor modifications. Briefly, P1 pups were anesthetized by
531 hypothermia. A glass micropipette was inserted into the lateral ventricle, and 2 μ l of plasmid
532 solution (concentration 3 μ g/ μ l) was injected by expiratory pressure using an aspirator tube
533 assembly (Drummond). Successfully injected animals were subjected to five 95V electrical
534 pulses (50 ms, separated by 950 ms intervals) using the CUY21 edit device (Nepagene,
535 Chiba, Japan), and 10 mm tweezer electrodes (CUY650P10, Nepagene) coated with
536 conductive gel (Signagel, Parker laboratories). Electroporated animals were reanimated in a
537 37°C incubator before returning to the mother.

538

539 Statistical analyses of mouse experiments

540 Analysis of CDC20B signal intensity in deuterosomes (graph in Fig. 3b). For each
541 category, >25 cells from two different animals were analyzed. Deuterosome regions were
542 delineated based on FOP staining and the intensity of CDC20B fluorescent immunostaining

543 was recorded using ImageJ software, and expressed as arbitrary units. Unpaired t test vs
544 immature: $p=0,0005$ (intermediate,***); $p<0,0001$ (Mature, ****).

545 Analysis of *Cdc20b* shRNAs efficiency (Fig. 4c): For each cell at the deuterosomal stage, the
546 intensity of CDC20B fluorescent immunostaining was recorded using ImageJ software and
547 expressed as arbitrary units. Data are mean \pm sem. Two independent experiments were
548 analyzed. A minimum of 35 cells per condition was analyzed. $n= 3, 4, 5$ and 5 animals for sh
549 control, sh273, sh274 and sh277, respectively. Unpaired t test vs sh control: $p<0.0001$ (sh273,
550 sh274 and sh277 ****).

551 Analysis of the number of FOXJ1 positive cells at 5dpe (Fig. 4d): Unpaired t test vs sh
552 control: 0.3961 (sh273, ns), 0.1265 (sh274, ns), 0.3250 (sh277, ns).

553 Analysis of the number of cells with non-disengaged centrioles at 9dpe (Fig. 4g): 15-20 fields
554 were analyzed per condition. $n= 4, 4, 3,$ and 4 animals for sh control, sh273, sh274 and sh277,
555 respectively, from 2 independent experiments. Unpaired t test vs sh control: $p<0.0001$ (sh273,
556 sh274, sh277 ****).

557 Analysis of the number of centrioles per cell at 15dpe (Fig. 4j): >100 cells were analyzed per
558 condition. $n= 3, 3, 3,$ and 3 animals for sh control, sh273, sh274 and sh277, respectively, from
559 2 independent experiments. Unpaired t test vs sh control: $p<0.0001$ (sh273, sh274, sh277
560 ****).

561 Analysis of ependymal cell categories at 15dpe (Fig. 4k): Data are mean \pm sem from three
562 independent experiments. More than 500 cells were analyzed for each condition. $n= 4, 4, 3,$
563 and 3 animals for sh control, sh273, sh274 and sh277, respectively. Unpaired t test vs sh
564 control: $p= 0.0004$ (sh273, ***), 0.0001 (sh274, ****), 0.0038 (sh277, **).

565

566 Mouse tracheal epithelial cells (MTECs)

567 MTECs cell cultures were established from the tracheas of 12 weeks-old mice. After
568 dissection, tracheas were placed in cold DMEM:F-12 medium (1:1) supplemented with 15
569 mM HEPES, 100 U/mL penicillin, 100 µg/mL streptomycin, 50 µg/mL gentamicin sulfate,
570 and 2.5 µg/ml amphotericin B. Each trachea was processed under a binocular microscope to
571 remove as much conjunctive tissue as possible with small forceps and was opened
572 longitudinally with small dissecting scissors. Tracheas were then placed in supplemented
573 DMEM:F-12 containing 0.15% protease XIV from *Streptomyces Griseus*. After overnight
574 incubation at 4°C, FCS was added to a final concentration of 10%, and tracheal epithelial
575 cells were detached by gentle agitation. Cells were centrifuged at 400g for 10 min and
576 resuspended in supplemented DMEM:F-12 containing 10% FCS. Cells were plated on regular
577 cell culture plates and maintained in a humidified atmosphere of 5% CO₂ at 37°C for 4 hours
578 to allow attachment of putative contaminating fibroblast. Medium containing cells in
579 suspension was further centrifuged at 400g for 5 min and cells were resuspended in
580 supplemented DMEM:F-12 containing BEGM Singlequots kit supplements and 5% FCS.
581 Cells were plated on rat tail collagen I-coated Transwell®. Typically, 5 tracheas resulted in 12
582 Transwells®. Medium was changed every other day. Air-liquid interface culture was
583 conducted once transepithelial electrical resistance had reached a minimum of 1000 ohm/cm²
584 (measured with EVOM2, World Precision Instruments).

585 Air-liquid interface culture was obtained by removing medium at the apical side of the
586 Transwell®, and by replacing medium at the basal side with supplemented DMEM:F-12
587 containing 2% Ultrosor-GTM (Pall Corporation). 10 µM DAPT (N-[N-(3,5-
588 difluorophenacetyl)-L- alanyl]-S-phenylglycine t-butyl ester) (Sigma) was added one day
589 after setting-up the air-liquid interface.

590

591 Immunostaining on HAECs and MTECs

592 Three days after setting-up the air-liquid interface, MTECs on Transwell membranes were
593 pre-extracted with 0.5% Triton X-100 in PBS for 3 min, and then fixed with 4%
594 paraformaldehyde in PBS for 15 min at room temperature. HAECs were treated 21 days after
595 setting-up the air-liquid interface. They were fixed directly on Transwells® with 100% cold
596 methanol for 10 min at -20°C (for CDC20B and Centrin2 co-staining, Supplementary Figure
597 4a,b) or with 4% paraformaldehyde in PBS for 15 min at room temperature (for CDC20B
598 single staining, Supplementary Figure 4c). All cells were then permeabilized with 0.5%
599 Triton X-100 in PBS for 5 min and blocked with 3% BSA in PBS for 30 min. The incubation
600 with primary and secondary antibodies was carried out at room temperature for 2 h and 1 h,
601 respectively. Nuclei were stained with 4,6-diamidino-2-phenylindole (DAPI). Transwell®
602 membranes were cut with a razor blade and mounted with ProLong Gold medium
603 (Thermofisher). Primary antibodies: rabbit anti-CDC20B (1:500; Proteintech, [133376-1-AP](#)),
604 rabbit anti-DEUP1 (1:500; Proteintech, [24579-1-AP](#)), anti-Centrin2 (Clone 20H5, 1:500;
605 Millipore, [04-1624](#)). Secondary antibodies: Alexa Fluor 488 goat anti-rabbit (1:1000; Thermo
606 Fisher Scientific, [A-11034](#)), Alexa Fluor 647 goat anti-mouse (1:1000; Thermo Fisher
607 Scientific, [A-21235](#)). For co-staining of CDC20B and DEUP1, CDC20B primary antibody
608 was directly coupled to CFTM 633 with the Mix-n-StainTM kit (Sigma-Aldrich) according to
609 the manufacturer's instruction. Coupled primary antibody was applied after secondary
610 antibodies had been extensively washed and after a 30 min blocking stage in 3% normal
611 rabbit serum in PBS.

612

613 Western blot and immunofluorescence on transfected cells

614 Cos1 or Hela cells were grown in DMEM supplemented with 10% heat inactivated FCS
615 and transfected with Fugene HD (Roche Applied Science) according to manufacturer's
616 protocol. Transfected or control cells were washed in PBS and lysed in 50 mM Tris-HCl pH

617 7.5, 150 mM NaCl, 1mM EDTA, containing 1% NP-40 and 0.25% sodium deoxycholate
618 (modified RIPA) plus a Complete Protease Inhibitor Cocktail (Roche Applied Science) on
619 ice. Cell extracts separated on polyacrylamide gels were transferred onto Optitran membrane
620 (Whatman) followed by incubation with rabbit anti-mouse CDC20B (1:500, Proteintech,
621 24579-1-AP) or homemade rabbit anti-*Xenopus* Cdc20b (1:300) antibody and horseradish
622 peroxidase conjugated secondary antibody (Jackson ImmunoResearch Laboratories, 711-035-
623 152 and 715-035-150). Signal obtained from enhanced chemiluminescence (Western
624 Lightning ECL Pro, Perkin Elmer) was detected with MyECL Imager (Thermo Fisher
625 Scientific).

626 For immunofluorescence staining, transfected cells were grown on glass coverslips and fixed
627 for 6 min in methanol at -20°C. Cells were washed in PBS, blocked in PBS, 3% BSA and
628 stained with rabbit anti-*Xenopus* Cdc20b (1:300) or rabbit anti-CFTR (1:200, Santa-Cruz
629 Biotechnology, 10747) as a negative control, in blocking buffer. After washings in PBS 0.1%
630 Tween-20, cells were incubated with Alexa fluor 488 donkey anti-rabbit antibody (Thermo
631 Fisher Scientific, R37118), washed, and DNA was stained with 250 ng/ml DAPI. Coverslip
632 were then rinsed and mounted in Prolong Gold antifade reagent (ThermoFisher Scientific) and
633 confocal images were acquired by capturing Z-series with 0.3 µm step size on a Zeiss LSM
634 510 laser scanning confocal microscope.

635

636 Co-immunoprecipitation studies

637 Asynchronous HEK cells were rinsed on ice with chilled Ca⁺⁺ and Mg⁺⁺ free Dulbecco's
638 PBS (DPBS, Invitrogen), harvested using a cell scraper and lysed on ice for 5 min in lysis
639 buffer (0.025M Tris, 0.15M NaCl, 0.001M EDTA, 1% NP-40, 5% glycerol; pH 7.4)
640 supplemented with EDTA and Halt™ Protease and Phosphatase Inhibitor Cocktail (Pierce,
641 ThermoFisher). Lysates were clarified (12000g, 4°C, 10 min) and the protein concentrations

642 were determined using the Bradford assay (Bio-Rad). Immunoprecipitations were performed
643 with the Pierce co-immunoprecipitation kit (Pierce, Thermofisher) according to the
644 manufacturer's instructions. For each immunoprecipitation, 1-1.5 mg of total lysate was
645 precleared on a control column, then incubated on columns coupled with 20 μ g of anti-GFP
646 or anti-c-myc-antibody (clone 9E10). Incubation was performed overnight at 4°C. Columns
647 were washed and eluted with 50 μ L elution buffer. Samples were denatured at 70°C for 10
648 min with Bolt™ LDS Sample Buffer and Bolt reducing agent, then separated on 4-12%
649 gradient Bolt precast gels (Thermofisher), transferred onto nitrocellulose (Millipore), and
650 subjected to immunoblot analysis using either anti-CDC20B (ProteinTech, 133376-1-AP) or
651 anti-c-myc antibody (clone 9E10). In Figure 6, note that the high level of expression of myc-
652 PLK1 (a) and myc-SPAG5 (b) drained out locally the ECL reagent at the peak of the protein.
653 The resulting double bands correspond in fact to unique ones. Human SPAG5, subcloned into
654 pCMV6-MT, was from OriGene. Human DEUP1 and PLK1 were cloned into pCS2-MT
655 vector (Addgene). Human CDC20B was cloned into pEGFP-C1, pEGFP-N1 (Clontech) for
656 the GFP fusion protein and pIRES-EYFP (Addgene) for the untagged protein.

657

658 In-Gel digestion, NanoHPLC, and Q-exactiveplus analysis

659 For mass spectrometry analysis, protein spots were manually excised from the gel and
660 destained with 100 μ L of H₂O/ACN (1/1). After 10 min vortexing, liquid was discarded, and
661 the procedure was repeated 2 times. They were rinsed with acetonitrile and dried under
662 vacuum. Extracts were reduced with 50 μ L of 10 mM dithiothreitol for 30 min at 56 °C, then
663 alkylated with 15 μ L of 55 mM iodoacetamide for 15 min at room temperature in the dark.
664 They were washed successively by: i) 100 μ L of H₂O/ACN (1/1) (2 times) and ii) 100 μ L of
665 acetonitrile. Gel pieces were rehydrated in 60 μ L of 50 mM NH₄HCO₃ containing 10 ng/ μ L
666 of trypsin (modified porcine trypsin, sequence grade, Promega) incubated for one hour at 4°C.

667 After the removal of trypsin, samples were incubated overnight at 37°C. Tryptic peptides
668 were extracted with: i) 60 µL of 1% FA (formic acid) in water (10 min at RT), ii) 60 µL
669 acetonitrile (10 min at RT). Extracts were pooled, concentrated under vacuum, resuspended in
670 15 µL of aqueous 0.1% formic acid for NanoHPLC separation.

671 Separation was carried out using a nanoHPLC (Ultimate 3000, Thermo Fisher Scientific).
672 After concentration on a µ-Precolumn Cartridge Acclaim PepMap 100 C₁₈ (i.d. 5 mm, 5 µm,
673 100 Å, Thermo Fisher Scientific) at a flow rate of 10 µL/min, using a solution of
674 H₂O/ACN/FA 98%/2%/0.1%, a second peptide separation was performed on a 75 µm i.d. x
675 250 mm (3 µm, 100 Å) Acclaim PepMap 100 C₁₈ column (Thermo Fisher Scientific) at a flow
676 rate of 300 nL/min. Solvent systems were: (A) 100% water, 0.1% FA, (B) 100% acetonitrile,
677 0.08% FA. The following gradient was used t = 0min 6% B; t = 3 min 6%B; t = 119min, 45%
678 B; t = 120 min, 90% B; t = 130 min 90% B (temperature at 35°C).

679 NanoHPLC was coupled via a nanoelectrospray ionization source to the Hybrid Quadrupole-
680 Orbitrap High Resolution Mass Spectrometer (Thermo Fisher Scientific). MS spectra were
681 acquired at a resolution of 70 000 (200 m/z) in a mass range of 300–2000 m/z with an AGC
682 target 3e6 value of and a maximum injection time of 100ms. The 10 most intense precursor
683 ions were selected and isolated with a window of 2m/z and fragmented by HCD (Higher
684 energy C-Trap Dissociation) with normalized collision energy (NCE) of 27. MS/MS spectra
685 were acquired in the ion trap with an AGC target 2e5 value, the resolution was set at 17 500 at
686 200 m/z combined with an injection time of 100 ms.

687 Data were reprocessed using Proteome Discoverer 2.1 equipped with Sequest HT. Files were
688 searched against the Swissprot Homo sapiens FASTA database (update of February 2016). A
689 mass accuracy of ± 10 ppm was used to precursor ions and 0.02 Da for product ions. Enzyme
690 specificity was fixed to trypsin, allowing at most two miscleavages. Because of the previous
691 chemical modifications, carbamidomethylation of cysteines was set as a fixed modification

692 and only oxydation of methionine was considered as a dynamic modification. Reverse decoy
693 databases were included for all searches to estimate false discovery rates, and filtered using
694 the Percolator algorithm at a 1% FDR.

695

696 *Xenopus* embryo injections, plasmids, RNAs, and morpholinos

697 Eggs obtained from NASCO females were fertilized *in vitro*, dejellied and cultured using
698 standard protocols⁵⁴. All injections were done at the 8-cell stage in one animal-ventral
699 blastomere (presumptive epidermis), except for electron microscopy analysis for which both
700 sides of the embryo was injected, and for RT-PCR analysis for which 2-cell embryos were
701 injected.

702 *cdc20b* riboprobe was generated from *Xenopus laevis* cDNA. Full-length sequence was
703 subcloned in pGEM™-T Easy Vector Systems (Promega). For sense probe it was linearized
704 by SpeI and transcribed by T7. For antisense probe it was linearized by ApaI and transcribed
705 by Sp6 RNA polymerase. Synthetic capped mRNAs were produced with the Ambion
706 mMMESSAGE mMACHINE Kit. pCS105/GFP-CAAX was linearized with AseI and mRNA
707 was synthesized with Sp6 polymerase. pCS2-mRFP and pCS2-GFP-gpi were linearized with
708 NotI and mRNA was synthesized with Sp6 polymerase. pCS-Centrin4-YFP (a gift from
709 Reinhard Köster, Technische Universität Braunschweig, Germany) was linearized with NotI
710 and mRNA was synthesized with Sp6 polymerase. pCS2-GFP-Deup1 and pCS2-
711 Multicilin(MCI)-hGR were kindly provided by Chris Kintner; both plasmids were linearized
712 with ApaI, and mRNAs were synthesized with Sp6 polymerase. Embryos injected with *MCI*-
713 *hGR* mRNA were cultured in Dexamethasone 20µM in MBS 0,1X from st11 until fixation.
714 pCS2-Separase wild-type and phosphomutant 2/4 (protease dead, PD) were provided by Marc
715 Kirchner and Olaf Stemann, respectively; plasmids were linearized with NotI and mRNAs
716 were synthesized with Sp6 polymerase. *Venus-cdc20b*, *cdc20b-Venus* and *cdc20b* were

717 generated by GATEWAY™ Cloning Technology (GIBCO BRL) from *Xenopus laevis cdc20b*
718 cDNA. *cdc20b* was also subcloned in pCS2-RFP to make *RFP-cdc20b* and *cdc20b-RFP*
719 fusions. All *cdc20b* constructs were linearized with NotI and mRNAs were synthesized with
720 Sp6 polymerase. Quantities of mRNA injected: 500pg for *GFP-CAAX*, *RFP*, *GFP-gpi*,
721 *Separase* and *Separase(PD)*; 25 to 500pg for *GFP-Deup1*; 40 to 500pg for *MCI-hGR*; 1ng
722 for *Venus-cdc20b*, *cdc20b-Venus*, *cdc20b*, and *cdc20b-RFP*; 500pg to 1ng for *RFP-cdc20b*.
723 Two independent morpholino antisense oligonucleotides were designed against *cdc20b*
724 (GeneTools, LLC). *cdc20b* ATG Mo: 5'-aaatcttctctaacttccagtcacat-3', *cdc20b* Spl Mo 5'-
725 acacatggcacaacgtaccacacatc-3'. 20ng of MOs was injected per blastomere or 10ng of each Mo
726 for co-injection.

727

728 PCR and Quantitative RT-qPCR

729 *Xenopus* embryos were snap frozen at different stages and stored at -80°C. Total RNAs were
730 purified with a Qiagen RNeasy kit (Qiagen). Primers were designed using Primer-BLAST
731 Software. PCR reactions were carried out using GoTaq® G2 Flexi DNA Polymerase
732 (Promega). RT reactions were carried out using iScript™ Reverse Transcription Supermix for
733 RT-qPCR (BIO-RAD). qPCR reactions were carried out using SYBRGreen on a CFX Biorad
734 qPCR cycler. To check *cdc20b* temporal expression by qPCR we directed primers to exons
735 9/10 junction (Forward: 5'-ggctatgaattggtgccccg-3') and exons 10/11 junction (Reverse: 5'-
736 gcagggagcagatctggg-3') to avoid amplification from genomic DNA. The relative expression
737 of *cdc20b* was normalized to the expression of the housekeeping gene *ornithine*
738 *decarboxylase* (*ODC*) for which primers were as follows: forward: 5'-
739 gccattgtgaagactctctccattc-3': reverse: 5'-ttcgggtgattccttgccac-3'.

740 To check the efficiency of Mo SPL, expected to cause retention of intron1 in the mature
741 mRNA of *cdc20b* we directed forward (5'-cctcccagagtagtagga-3') and reverse (5'-
742 gcatgtgtactttctgctcca-3') primers in exon1 and exon2, respectively.

743 To check the expression of *p53* in morphants by qPCR, primers were as follows: forward: 5'-
744 cgcagccgctatgagatgatt-3'; reverse: 5'-cacttgccgcacttaatggt-3'. The relative expression of *p53*
745 was normalized to Histone4 expression (H4) for which primers were as follows: forward: 5'-
746 ggtgatgccctggatgtgt-3'; reverse: 5'-ggcaaaggaggaaaaggactg-3'.

747

748 Immunostaining on *Xenopus* embryos

749 Embryos were fixed in 4% paraformaldehyde (PFA) overnight at 4°C and stored in 100%
750 methanol at -20°C. Embryos were rehydrated in PBT and washed in MABX (Maleic Acid
751 Buffer + Triton X100 0,1% v/v). Next, embryos were incubated in Blocking Reagent (Roche)
752 2% BR + 15% Serum + MABX with respective primary and secondary antibodies. The anti-
753 *Xenopus laevis* CDC20B antibody was obtained by rabbit immunization with the peptide
754 SPDQRRIFSAAANGT (amino acids 495–509) conjugated to keyhole limpet hemocyanin,
755 followed by affinity purification (Eurogentec). For immunofluorescence, embryos were fixed
756 at RT in PFA 4% in PBS, and incubated in the CDC20B antibody diluted 1/150 in BSA 3% in
757 PBS. For all experiments secondary antibodies conjugated with Alexa were used. **GFP-
758 CAAX in Supplementary Figure 5g was revealed using a rabbit anti-GFP antibody together
759 with a secondary antibody coupled to Alkaline Phosphatase (AP), which was revealed as
760 follows: embryos incubated with the AP-conjugated antibody were washed twice in alkaline
761 phosphatase buffer (PAB) (NaCl 0.1M, Tris HCl pH 9.5 0.1M, MgCl₂ 0.05M, Tween 0.1%),
762 10 minutes each. Next, embryos were incubated in PAB with INT/BCIP substrate (Roche,
763 REF:11681460001) until appropriate staining. Finally embryos were washed twice in MABX
764 and fixed in MEMFA 30min at RT.** To mark cortical actin in MCCs, embryos were fixed in

765 4% paraformaldehyde (PFA) in PBT (PBS + 0,1% Tween v/v) for 1h at room temperature
766 (RT), washed 3x10 min in PBT at RT, then stained with phalloidin-Alexa Fluor 555
767 (Invitrogen, 1:40 in PBT) for 4 h at RT, and washed 3x10 min in PBT at RT. Primary
768 antibodies: mouse anti-Acetylated- α -Tubulin (Clone 6-11B-1, Sigma-Aldrich, T7451,
769 1:1000), rabbit anti- γ -Tubulin (Abcam, Ab 16504, 1:500), mouse anti- γ -Tubulin (Clone
770 GTU88, Ab 11316, Abcam, 1:500), Chicken anti-GFP (AVES, GFP-1020, 1:1000), rabbit
771 anti-GFP (Torrey Pines Biolabs, TP401, 1:500), mouse anti-Centrin (Clone 20H5, EMD
772 Millipore, 04-1624, 1:500). Secondary antibodies: donkey anti-rabbit-AP (Jackson
773 ImmunoResearch, 711055152, 1:1000), Alexa Fluor 647 goat anti-mouse IgG2a (1:500;
774 Thermo Fisher Scientific, A-21241), Alexa Fluor 488 goat anti-chicken (1:500; Thermo
775 Fisher Scientific, A-11039), Alexa Fluor 568 goat anti-rabbit (1:500; Thermo Fisher
776 Scientific, A-11011).

777

778 *In situ* hybridization on *Xenopus* embryos

779 Whole-mount chromogenic *in situ* hybridization and whole-mount fluorescent *in situ*
780 hybridization (FISH) was performed as detailed by Marchal and colleagues⁵⁴, and Castillo-
781 Briceno and Kodjabachian⁵⁵, respectively. For single staining, all RNA probes were labeled
782 with digoxigenin. For FISH on section, embryos were fixed in 4% paraformaldehyde (PFA),
783 stored in methanol for at least 4 h at -20°C , then rehydrated in PBT (PBS + Tween 0.1% v/v),
784 treated with triethanolamine and acetic anhydride, incubated in increasing sucrose
785 concentrations and finally embedded with OCT (VWR Chemicals). 12 μm -thick cryosections
786 were made. Double FISH on sections was an adaptation of the whole-mount FISH method.
787 80ng of *cdc20b* digoxigenin-labeled sense and antisense riboprobes and 40ng of antisense α -
788 *tubulin* fluorescein-labeled riboprobe⁵⁶ were used for hybridization. All probes were
789 generated from linearized plasmids using RNA-labeling mix (Roche). FISH was carried out

790 using Tyramide Signal Amplification – TSA™ Plus Cyanine 3/Fluorescein System
791 (PerkinElmer). Antibodies: Anti-DigAP (Roche, 11266026, 1:5000), Anti-DigPOD (Roche,
792 11207733910, 1:500), Anti-FluoPOD (Roche, 11426346910, 1:500).

793

794 Microscopy

795 Confocal: Flat-mounted epidermal explants were examined with a Zeiss LSM 780 confocal
796 microscope. Four-colors confocal z-series images were acquired using sequential laser
797 excitation, converted into single plane projection and analyzed using ImageJ software.

798 Scanning Electron Microscopy (SEM): stage 37 *Xenopus* embryos were fixed in 3%
799 glutaraldehyde in 0.1 M phosphate buffer pH 7.4 (19 ml monosodium phosphate 0.2 M and
800 81 ml disodium phosphate 0.2 M) made with filtered (0.22 µm) bi-distilled water, during 4 h
801 with vigorous agitation, then washed with phosphate buffer and filtered bi-distilled water,
802 to be successively dehydrated in ethanol at 25, 50 and 70% for 30 minutes each; then,
803 embryos were stored in fresh ethanol 70% at 4°C for 1–2 days before further processing.
804 Embryos in 70% ethanol were further dehydrated with vigorous agitation in ethanol once at
805 90% and twice at 100% for 30 minutes each; they were subsequently subjected to CO₂ critical
806 point drying (CPD030, Balzers) at 31°C and 73 atm. Finally, samples were sputter-coated
807 with gold (vacuum 1×10⁻¹² Torr, beam energy 3–4 keV) for immediate SEM digital imaging
808 (FEI TENE0) of the skin epidermis. Transmission Electron Microscopy (TEM): stage 25
809 *Xenopus* embryos were fixed overnight at 4°C in 2.5% glutaraldehyde, 2% paraformaldehyde,
810 0.1% tannic acid in a sodium cacodylate buffer 0.05 M pH7.3. Next, embryos were washed
811 3x15 min in cacodylate 0.05 M at 4°C. Post-fixation was done in 1% osmium buffer for 2 h.
812 Next, embryos were washed in buffer for 15 min. Then, embryos were washed in water and
813 dehydrated conventionally with alcohol, followed by a step in 70% alcohol containing 2%
814 uranyl during 1 to 2 h at RT, or overnight at 4°C. Following 3 incubations in 100% alcohol,

815 completed with 3 washes of acetone, embryos were included in classical epon resin, which
816 was polymerized in oven at 60°C for 48 h. Sections of 80 nm were made and analyzed into an
817 FMI TECNAI microscope with acceleration of 200kV.

818

819 Statistical analysis of *Xenopus* experiments

820 To quantify the effect of our different experiments, we applied One-way ANOVA analysis
821 and Bonferroni's multiple comparisons test (t test). ***P<0.05; ns = not significant. Statistical
822 analyses were done using GraphPad Prism 6.

823 Fig. 5o and Fig. S6k: 10 cells per condition were analyzed and the total number of Centrin-
824 YFP or γ -tubulin positive spots per injected cell was counted.

825 Fig. 7g: 5 fields (20x zoom) per condition were analyzed, and the total number of properly
826 ciliated MCCs based on acetylated α -tubulin staining among GFP positive cells per field was
827 counted. Each field corresponded to a different embryo.

828 Fig. 5s : 160-200 cells per condition were analyzed. n= 6, 8, and 10 embryos from 3
829 independent experiments for control, Mo ATG and Mo Spl, respectively. Unpaired t test vs
830 control: p=0,0037 (Mo ATG **) and 0,0004 (Mo Spl ***).

831

832 Data availability statement

833 scRNAseq data was submitted to the GEO portal under series reference GSE103518. All
834 other relevant data are available from the authors.

835

836 **References**

837 1. Meunier, A. & Azimzadeh, J. Multiciliated Cells in Animals. *Cold Spring Harb*
838 *Perspect Biol* **8** (2016).

- 839 2. Spassky, N. & Meunier, A. The development and functions of multiciliated epithelia.
840 *Nat Rev Mol Cell Biol* **18**, 423-436 (2017).
- 841 3. Brooks, E.R. & Wallingford, J.B. Multiciliated cells. *Curr Biol* **24**, R973-982 (2014).
- 842 4. Kyrousi, C. *et al.* Mcidas and GemC1 are key regulators for the generation of
843 multiciliated ependymal cells in the adult neurogenic niche. *Development* **142**, 3661-3674
844 (2015).
- 845 5. Arbi, M. *et al.* GemC1 controls multiciliogenesis in the airway epithelium. *EMBO Rep*
846 **17**, 400-413 (2016).
- 847 6. Terre, B. *et al.* GEMC1 is a critical regulator of multiciliated cell differentiation.
848 *EMBO J* **35**, 942-960 (2016).
- 849 7. Zhou, F. *et al.* Gmnc Is a Master Regulator of the Multiciliated Cell Differentiation
850 Program. *Curr Biol* **25**, 3267-3273 (2015).
- 851 8. Stubbs, J.L., Vldar, E.K., Axelrod, J.D. & Kintner, C. Multicilin promotes centriole
852 assembly and ciliogenesis during multiciliate cell differentiation. *Nat Cell Biol* **14**, 140-147
853 (2012).
- 854 9. Ma, L., Quigley, I., Omran, H. & Kintner, C. Multicilin drives centriole biogenesis via
855 E2f proteins. *Genes Dev* **28**, 1461-1471 (2014).
- 856 10. Quigley, I.K. & Kintner, C. Rfx2 Stabilizes Foxj1 Binding at Chromatin Loops to
857 Enable Multiciliated Cell Gene Expression. *PLoS Genet* **13**, e1006538 (2017).
- 858 11. Chung, M.I. *et al.* RFX2 is broadly required for ciliogenesis during vertebrate
859 development. *Dev Biol* **363**, 155-165 (2012).
- 860 12. Boon, M. *et al.* MCIDAS mutations result in a mucociliary clearance disorder with
861 reduced generation of multiple motile cilia. *Nat Commun* **5**, 4418 (2014).
- 862 13. Wallmeier, J. *et al.* Mutations in CCNO result in congenital mucociliary clearance
863 disorder with reduced generation of multiple motile cilia. *Nat Genet* **46**, 646-651 (2014).

- 864 14. Sorokin, S.P. Reconstructions of centriole formation and ciliogenesis in mammalian
865 lungs. *J Cell Sci* **3**, 207-230 (1968).
- 866 15. Dirksen, E.R. Centriole morphogenesis in developing ciliated epithelium of the mouse
867 oviduct. *J Cell Biol* **51**, 286-302 (1971).
- 868 16. Anderson, R.G. & Brenner, R.M. The formation of basal bodies (centrioles) in the
869 Rhesus monkey oviduct. *J Cell Biol* **50**, 10-34 (1971).
- 870 17. Kalnins, V.I. & Porter, K.R. Centriole replication during ciliogenesis in the chick
871 tracheal epithelium. *Z Zellforsch Mikrosk Anat* **100**, 1-30 (1969).
- 872 18. Steinman, R.M. An electron microscopic study of ciliogenesis in developing epidermis
873 and trachea in the embryo of *Xenopus laevis*. *Am J Anat* **122**, 19-55 (1968).
- 874 19. Al Jord, A. *et al.* Centriole amplification by mother and daughter centrioles differs in
875 multiciliated cells. *Nature* **516**, 104-107 (2014).
- 876 20. Klos Dehring, D.A. *et al.* Deuterosome-mediated centriole biogenesis. *Dev Cell* **27**,
877 103-112 (2013).
- 878 21. Zhao, H. *et al.* The Cep63 paralogue Deup1 enables massive de novo centriole
879 biogenesis for vertebrate multiciliogenesis. *Nat Cell Biol* **15**, 1434-1444 (2013).
- 880 22. Sir, J.H. *et al.* A primary microcephaly protein complex forms a ring around parental
881 centrioles. *Nat Genet* **43**, 1147-1153 (2011).
- 882 23. Marcet, B. *et al.* Control of vertebrate multiciliogenesis by miR-449 through direct
883 repression of the Delta/Notch pathway. *Nat Cell Biol* **13**, 693-699 (2011).
- 884 24. Tan, F.E. *et al.* Myb promotes centriole amplification and later steps of the
885 multiciliogenesis program. *Development* **140**, 4277-4286 (2013).
- 886 25. Yu, H. Cdc20: a WD40 activator for a cell cycle degradation machine. *Mol Cell* **27**, 3-
887 16 (2007).

- 888 26. Song, R. *et al.* miR-34/449 miRNAs are required for motile ciliogenesis by repressing
889 cp110. *Nature* **510**, 115-120 (2014).
- 890 27. Otto, T. *et al.* Cell cycle-targeting microRNAs promote differentiation by enforcing
891 cell-cycle exit. *Proc Natl Acad Sci U S A* **114**, 10660-10665 (2017).
- 892 28. Wu, J. *et al.* Two miRNA clusters, miR-34b/c and miR-449, are essential for normal
893 brain development, motile ciliogenesis, and spermatogenesis. *Proc Natl Acad Sci U S A* **111**,
894 E2851-2857 (2014).
- 895 29. Chevalier, B. *et al.* miR-34/449 control apical actin network formation during
896 multiciliogenesis through small GTPase pathways. *Nat Commun* **6**, 8386 (2015).
- 897 30. Mercey, O. *et al.* Characterizing isomiR variants within the microRNA-34/449 family.
898 *FEBS Lett* **591**, 693-705 (2017).
- 899 31. Firat-Karalar, E.N., Rauniyar, N., Yates, J.R., 3rd & Stearns, T. Proximity interactions
900 among centrosome components identify regulators of centriole duplication. *Curr Biol* **24**,
901 664-670 (2014).
- 902 32. Robu, M.E. *et al.* p53 activation by knockdown technologies. *PLoS Genet* **3**, e78
903 (2007).
- 904 33. Werner, M.E. *et al.* Radial intercalation is regulated by the Par complex and the
905 microtubule-stabilizing protein CLAMP/Spel1. *J Cell Biol* **206**, 367-376 (2014).
- 906 34. Firat-Karalar, E.N. & Stearns, T. The centriole duplication cycle. *Philos Trans R Soc*
907 *Lond B Biol Sci* **369** (2014).
- 908 35. Tsou, M.F. *et al.* Polo kinase and separase regulate the mitotic licensing of centriole
909 duplication in human cells. *Dev Cell* **17**, 344-354 (2009).
- 910 36. Kim, J., Lee, K. & Rhee, K. PLK1 regulation of PCNT cleavage ensures fidelity of
911 centriole separation during mitotic exit. *Nat Commun* **6**, 10076 (2015).

- 912 37. Matsuo, K. *et al.* Kendrin is a novel substrate for separase involved in the licensing of
913 centriole duplication. *Curr Biol* **22**, 915-921 (2012).
- 914 38. Al Jord, A. *et al.* Calibrated mitotic oscillator drives motile ciliogenesis. *Science* **358**,
915 803-806 (2017).
- 916 39. Huttlin, E.L. *et al.* The BioPlex Network: A Systematic Exploration of the Human
917 Interactome. *Cell* **162**, 425-440 (2015).
- 918 40. Rual, J.F. *et al.* Towards a proteome-scale map of the human protein-protein
919 interaction network. *Nature* **437**, 1173-1178 (2005).
- 920 41. Thein, K.H., Kleylein-Sohn, J., Nigg, E.A. & Gruneberg, U. Astrin is required for the
921 maintenance of sister chromatid cohesion and centrosome integrity. *J Cell Biol* **178**, 345-354
922 (2007).
- 923 42. Chiu, S.C. *et al.* The mitosis-regulating and protein-protein interaction activities of
924 astrin are controlled by aurora-A-induced phosphorylation. *Am J Physiol Cell Physiol* **307**,
925 C466-478 (2014).
- 926 43. Eguren, M. *et al.* The APC/C cofactor Cdh1 prevents replicative stress and p53-
927 dependent cell death in neural progenitors. *Nat Commun* **4**, 2880 (2013).
- 928 44. Chung, H.J., Park, J.E., Lee, N.S., Kim, H. & Jang, C.Y. Phosphorylation of Astrin
929 Regulates Its Kinetochores Function. *J Biol Chem* **291**, 17579-17592 (2016).
- 930 45. Qiu, X. *et al.* Single-cell mRNA quantification and differential analysis with Census.
931 *Nat Methods* **14**, 309-315 (2017).
- 932 46. Macosko, E.Z. *et al.* Highly Parallel Genome-wide Expression Profiling of Individual
933 Cells Using Nanoliter Droplets. *Cell* **161**, 1202-1214 (2015).
- 934 47. Kim, D. *et al.* TopHat2: accurate alignment of transcriptomes in the presence of
935 insertions, deletions and gene fusions. *Genome Biol* **14**, R36 (2013).

- 936 48. Anders, S., Pyl, P.T. & Huber, W. HTSeq--a Python framework to work with high-
937 throughput sequencing data. *Bioinformatics* **31**, 166-169 (2015).
- 938 49. Love, M.I., Huber, W. & Anders, S. Moderated estimation of fold change and
939 dispersion for RNA-seq data with DESeq2. *Genome Biol* **15**, 550 (2014).
- 940 50. Langmead, B. & Salzberg, S.L. Fast gapped-read alignment with Bowtie 2. *Nat*
941 *Methods* **9**, 357-359 (2012).
- 942 51. Heinz, S. *et al.* Simple combinations of lineage-determining transcription factors
943 prime cis-regulatory elements required for macrophage and B cell identities. *Mol Cell* **38**,
944 576-589 (2010).
- 945 52. Boutin, C. *et al.* NeuroD1 induces terminal neuronal differentiation in olfactory
946 neurogenesis. *Proc Natl Acad Sci U S A* **107**, 1201-1206 (2010).
- 947 53. Boutin, C., Diestel, S., Desoeuvre, A., Tiveron, M.C. & Cremer, H. Efficient in vivo
948 electroporation of the postnatal rodent forebrain. *PLoS One* **3**, e1883 (2008).
- 949 54. Marchal, L., Luxardi, G., Thome, V. & Kodjabachian, L. BMP inhibition initiates
950 neural induction via FGF signaling and *Zic* genes. *Proc Natl Acad Sci U S A* **106**, 17437-
951 17442 (2009).
- 952 55. Castillo-Briceno, P. & Kodjabachian, L. *Xenopus* embryonic epidermis as a
953 mucociliary cellular ecosystem to assess the effect of sex hormones in a non-reproductive
954 context. *Front Zool* **11**, 9 (2014).
- 955 56. Deblandre, G.A., Wettstein, D.A., Koyano-Nakagawa, N. & Kintner, C. A two-step
956 mechanism generates the spacing pattern of the ciliated cells in the skin of *Xenopus* embryos.
957 *Development* **126**, 4715-4728 (1999).

958

959 **Acknowledgements**

960 We are grateful to Chris Kintner, Marc Kirschner, Olaf Stemmann, Reinhard Köster, Xavier
961 Morin and Xueliang Zhu for reagents. Imaging in IBDM was performed on PiCSL-FBI core
962 facility, supported by the French National Research Agency through the program
963 "Investments for the Future" (France-BioImaging, ANR-10-INBS-04). Sequencing at
964 UCAGenomiX (IPMC), a partner of the National Infrastructure France Génomique, was
965 supported by Commissariat aux Grands Investissements (ANR-10-INBS-09-03, ANR-10-
966 INBS-09-02) and Canceropôle PACA. The authors thank Florian Roguet for *Xenopus* care,
967 and Nathalie Garin from Leica Microsystems GmbH for technical advice on STED
968 microscopy. We are grateful to Rainer Waldmann, Kévin Lebrigand, Virginie Magnone and
969 Nicolas Nottet for fruitful discussions on single cell RNA sequencing, and Delphine Debayle
970 for help with mass spectrometry experiments. We thank Julien Royet and Harold Cremer for
971 insightful comments on the manuscript. This project was funded by grants from ANR (ANR-
972 11-BSV2-021-02, ANR-13-BSV4-0013, ANR-15-CE13-0003), FRM (DEQ20141231765,
973 DEQ20130326464, DEQ20180339158), Fondation ARC (PJA 20161204865, PJA
974 20161204542), the labex Signalife (ANR-11-LABX-0028-01), the association Vaincre la
975 Mucoviscidose (RF20140501158, RF20120600738, RF20150501288), and the Chan
976 Zuckerberg Initiative (Silicon Valley Foundation, 2017-175159 -5022). OM, CB and DRR were
977 supported by fellowships from Ligue Nationale contre le Cancer (OM and CB), and Fondation
978 ARC (DRR).

979

980 **Author contributions**

981 PB, BM and LK designed and supervised the study, and obtained funding. LEZ, SRG, OM
982 performed and analyzed human and mouse airway cells experiments. DRR and VT performed
983 and analyzed *Xenopus* experiments. CB performed and analyzed all experiments on mouse
984 ependymal MCCs and contributed to the description of *Xenopus* deuterosomes. OR

985 characterized CDC20B antibodies. MD and AP performed the bioinformatic analysis. NP
986 carried out scRNAseq experiments. ASG performed mass spectrometry analyses. GP
987 designed and performed CDC20B interaction studies. All authors were involved in data
988 interpretation. DRR, LEZ and CB designed the figures. LK drafted the original manuscript.
989 DRR, LEZ, CB, BM, PB and LK edited the manuscript.

990

991 **Competing financial interests**

992 The authors declare no competing interests.

993

994 **Figures and legends**

995

996 **Figure 1: Single-cell RNA-seq analysis reveals MCC transcriptome at deuterosome-**
997 **stage.**

998 (a) Experimental design of the scRNA-seq experiment. (b) tSNE plot. Each point is a
999 projection of a unique cell on a 2D space generated by the tSNE algorithm. Blue dots
1000 represent *MKI67*-positive proliferating cells, and red dots represent *DEUP1*-positive cells
1001 corresponding to maturing MCCs at deuterosome stage. (c) Cell cycle-related gene set
1002 expression in HAECs measured by scRNA-seq. Cells were ordered along a pseudotime axis,
1003 defined with the Monocle2 package. Phase specific scores are displayed in the top heatmap.
1004 Expression of selected genes is displayed in the bottom heatmap. (d) tSNEs plots for a
1005 selection of genes specifically enriched in deuterosome-stage cells. Note that *CDC20B*
1006 exhibits the most specific expression among deuterosome marker genes.

1007

1008 **Figure 2: Composition and organization of vertebrate deuterosomes**

1009 (a-b) Maturing mouse ependymal MCCs were immunostained as indicated, pictures were
1010 taken with confocal (a) or STED (b) microscope. (a) DEUP1 stains the deuterosome core
1011 (ring) and a close fibrous area that defines the perideuterosomal region. The centriolar marker
1012 FOP reveals procentrioles arranged in a circle around the deuterosome. Pericentrin (PCNT) is
1013 enriched in the perideuterosomal region. γ -Tubulin (γ -TUB) stains the core as well as the
1014 periphery of the deuterosome. (b) STED pictures showing the organization of FOP, PCNT
1015 and γ -TUB around deuterosomes. Individual centrioles identified by FOP staining are pointed
1016 out with arrowheads. The diagram was drawn from the adjacent FOP photograph to help
1017 reveal the regular concentric organization of nascent centrioles in a typical deuterosomal
1018 figure. (c) *Xenopus* embryos were immunostained for γ -Tubulin (γ -Tub) and Centrin and
1019 high-magnification pictures of immature epidermal MCCs were taken. In these cells, Centrin-
1020 positive procentrioles grow around γ -Tubulin positive structures. (d) *Xenopus* embryos were

1021 injected with *Multicilin-hGR* and *GFP-Deup1* mRNAs, treated with dexamethasone at
1022 gastrula st11 to induce Multicilin activity, and immunostained at neurula st18 for γ -Tubulin,
1023 GFP and Centrin. Scale bars: 5 μ m (**a**, top), 500nm (**a**, bottom), 500nm (**b**), 10 μ m (**c**, **d**, large
1024 view), 1 μ m (**c**, **d**, high magnification).

1025

1026 **Figure 3: CDC20B associates to vertebrate deuterosomes.**

1027 (**a**) Double immunofluorescence was performed on mouse tracheal MCCs after 3 days of
1028 culture in air-liquid interface. Low magnification confocal panels show coincident CDC20B
1029 and DEUP1 staining in several individual MCCs. High magnification on a single MCC
1030 reveals the prominent association of CDC20B to large deuterosomes marked by DEUP1
1031 (arrowheads). Note that some smaller deuterosomes do not contain CDC20B (arrows). (**b**)
1032 Mouse ependymal MCCs were immunostained as indicated, and high magnification confocal
1033 pictures of cells with immature and mature deuterosomal figures were taken. In these cells,
1034 centrioles revealed by FOP form a ring around deuterosomes. CDC20B staining forms a ring
1035 inside the ring of FOP-positive procentrioles indicating that CDC20B is tightly associated to
1036 deuterosomes. Note that the CDC20B signal associated to deuterosome increased with their
1037 maturation (high-magnification pictures of >25 cells per category from two different
1038 animals were quantified in the graph; horizontal bars are mean values and vertical lines are
1039 standard deviations). Unpaired t test vs immature: p=0,0005 (intermediate, ***); p<0,0001
1040 (mature, ****). (**c**) *Xenopus* embryos were injected with *GFP-Deup1* mRNA and
1041 immunostained at neurula st18 as indicated. Scale bars: 5 μ m (**a**, **b**, large view), 1.5 μ m (**a**,
1042 high magnification), 500nm (**b**, high magnification), 10 μ m (**c**).

1043

1044 **Figure 4: CDC20B knockdown impairs multiciliogenesis in mouse ependymal MCCs.**

1045 (a,b) Ependyma were stained for CDC20B (green) and FOXJ1 (nuclear MCC fate marker,
1046 red) 5 days post electroporation (5dpe) of control shRNA (a) or *Cdc20b* shRNA (b). sh277 is
1047 exemplified here, but all three *Cdc20b* shRNAs produced similar effects. (c) Graph showing
1048 the quantification of CDC20B protein levels in cells at the deuterosomal stage at 5dpe from
1049 two experiments. Horizontal lines are mean values and vertical lines are standard error mean.
1050 Unpaired t test: $p < 0.0001$ (sh273, sh274, sh277, ****). (d) Histogram showing the number of
1051 FOXJ1-positive nuclei observed for each field (dot), with mean values (horizontal lines) and
1052 standard deviations (vertical lines) from two experiments. Unpaired t test: 0.3961 (sh273, ns),
1053 0.1265 (sh274, ns), 0.3250 (sh277, ns). No significant variations were observed between
1054 conditions, indicating that MCC fate acquisition was not affected by *Cdc20b* knockdown. (e-
1055 f) Confocal pictures of 9dpe ependyma electroporated with control shRNA (e) or *Cdc20b*
1056 shRNAs (f) and stained for DEUP1 (deuterosome, green), FOP (centrioles, red) and ZO1 (cell
1057 junction, white). DEUP1 positive deuterosomes with non-disengaged FOP positive centrioles
1058 were observed much more frequently in MCCs electroporated with *Cdc20b* shRNAs
1059 compared to control. (g) Histogram showing the percentage of MCCs with non-disengaged
1060 centrioles per field (dots), with mean values (horizontal bars) and standard deviations (vertical
1061 lines). Two experiments were analyzed. Unpaired t test: $p < 0.0001$ (sh273, sh274, sh277,
1062 ****). (h-i) Confocal pictures of 15dpe ependyma stained for FOP (centrioles, green), α -
1063 Tubulin (α -TUB, cilia, red) and ZO1 (cell junction, white) showing the morphology of
1064 normal MCCs in shRNA control condition (h), and examples of defects observed in MCCs
1065 treated with sh *Cdc20b* (i). (j) Histogram showing the number of released centrioles per cell
1066 (dots), with mean values (horizontal bars) and standard deviations (vertical lines). (k) Bar
1067 graph showing the percentage of normal and abnormal MCCs. MCCs were scored abnormal
1068 when they did not display organized centriole patches associated to cilia. Three experiments

1069 were analyzed. Unpaired t test: $p=0.0004$ (sh273, ***), 0.0001 (sh274, ****), 0.0038 (sh277,
1070 **). Scale bars: $20\mu\text{m}$ (a), $5\mu\text{m}$ (e, i).

1071

1072 **Figure 5: *cdc20b* knockdown impairs multiciliogenesis in *Xenopus* epidermal MCCs.**

1073 (a-c) 8-cell embryos were injected in presumptive epidermis with *GFP-CAAX* mRNA and
1074 *cdc20b* morpholinos, as indicated. Embryos at tailbud st25 were processed for fluorescent
1075 staining against GFP (injection tracer, green) and Acetylated- α -Tubulin (Ac- α -Tub, cilia,
1076 white). White dotted lines indicate the position of orthogonal projections shown in bottom
1077 panels. Note that *cdc20b* morphant MCCs display cytoplasmic filaments but do not grow cilia
1078 (white arrowheads). (d-f) Scanning Electron Microscopy (SEM) of control (d) and *cdc20b*
1079 morphant (e,f) embryos at tadpole st31. Yellow arrowheads point at normal (d) and defective
1080 MCCs (e,f). (g-i) Transmission Electron Microscopy (TEM) of control (g) and *cdc20b*
1081 morphant (h,i) embryos at tailbud st25. Yellow arrowheads point at normally docked basal
1082 bodies supporting cilia (g) and undocked centrioles unable to support cilia (h,i). (j-n) 8-cell
1083 embryos were injected in presumptive epidermis with *centrin-YFP* mRNA, *cdc20b*
1084 morpholinos, and *cdc20b* mRNA, as indicated. Centrin-YFP fluorescence was observed
1085 directly to reveal centrioles (yellow). Nuclei were revealed by DAPI staining in blue. White
1086 dotted lines indicate the position of orthogonal projections shown in bottom panels. Yellow
1087 arrowheads point at undocked centrioles. (o) Bar graph showing the number of BBs per
1088 MCC, and standard error mean, as counted by Centrin-YFP dots. One way ANOVA and
1089 Bonferroni's Multiple Comparisons Test on two experiments, *** = $p<0.0001$. *cdc20b*
1090 knockdown significantly reduced the number of BBs per cell, and this defect could be
1091 corrected by *cdc20b* co-injection with Mo Spl. (p-u) Embryos were injected with *Multicilin-*
1092 *hGR* and *GFP-Deup1* mRNAs, treated with dexamethasone at gastrula st11 to induce
1093 Multicilin activity, and immunostained at neurula st23 against Acetylated- α -tubulin (cilia,

1094 white), GFP (deuterosomes, green) and Centrin (centrioles, red). **(p)** Control cells showed
1095 individual centrioles, many of which had initiated ciliogenesis. Note that Deup1-positive
1096 deuterosomes were no longer visible at this stage. **(q,r,t,u)** *cdc20b* morphant MCCs showed
1097 procentrioles still engaged on deuterosomes and lacked cilia. **(s)** bar graph showing the
1098 percentage of cells that completed or not centriole disengagement with standard deviations
1099 (vertical lines). Three experiments were analyzed. Unpaired t test: $p=0,0037$ (Mo ATG, **),
1100 $0,0004$ (Mo Spl, ***). Scale bars: $20\mu\text{m}$ (**a, d**), $1\mu\text{m}$ (**g, t**), $5\mu\text{m}$ (**j, p**).

1101

1102 **Figure 6: CDC20B interacts with PLK1, SPAG5 and DEUP1**

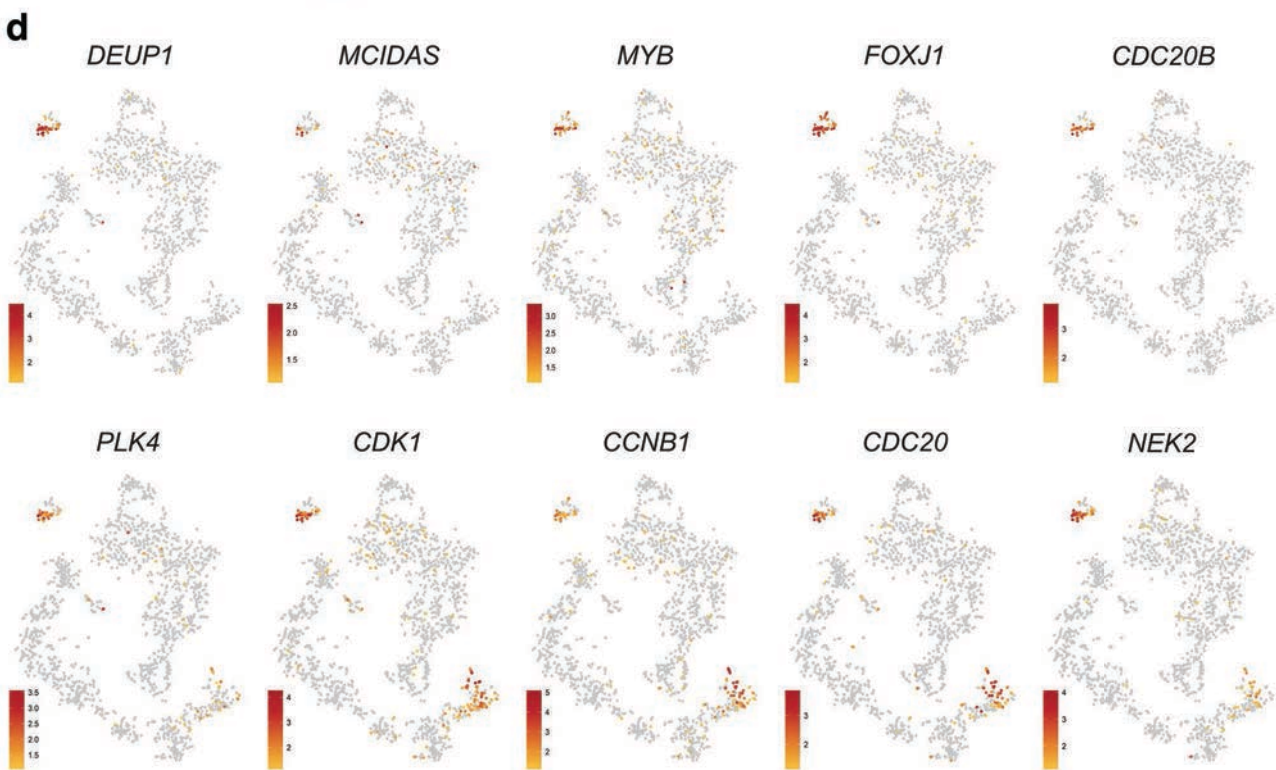
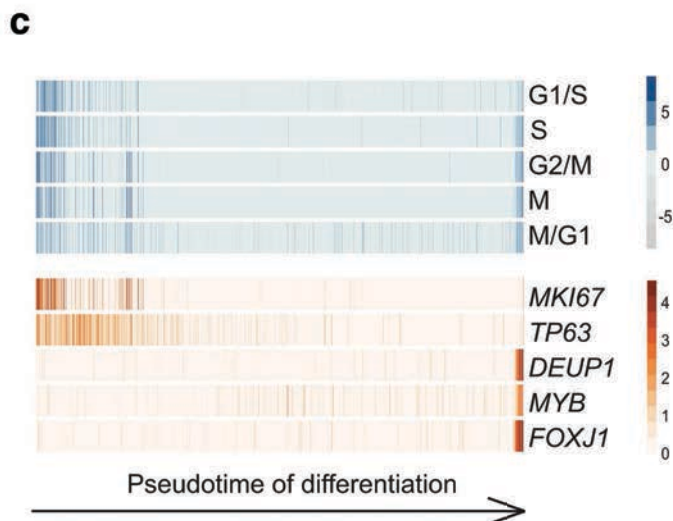
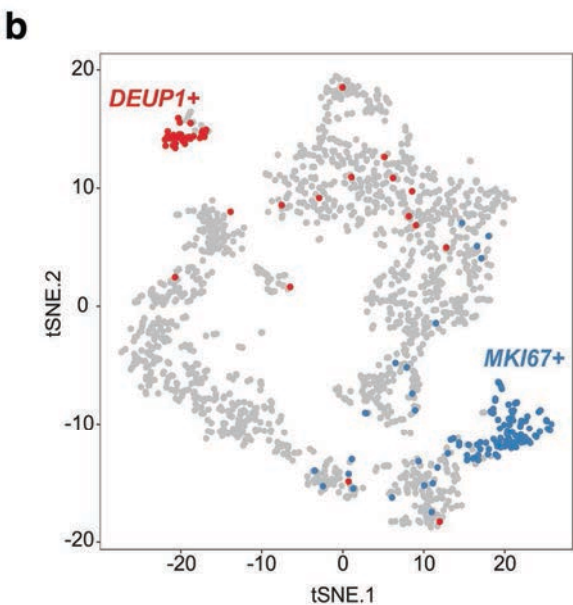
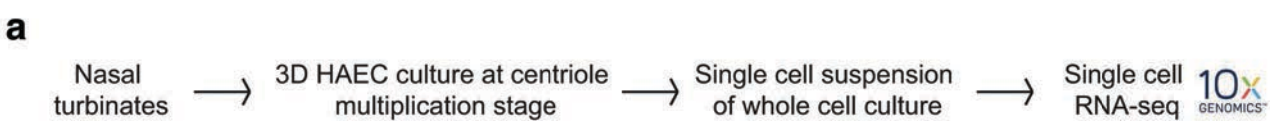
1103 **(a, c, e)** Co-immunoprecipitations of PLK1, SPAG5 and DEUP1 with CDC20B were tested
1104 after transfections of different constructs in HEK cells, indicated at the top of each panel.
1105 Proteins (left legend) were revealed by immunoblotting. **(b, d)** Maturing mouse ependyma
1106 were immunostained for the indicated proteins, and pictures were taken with a confocal
1107 microscope. PLK1 and SPAG5 are expressed in maturing MCCs. High magnifications show
1108 that PLK1 is enriched in the perideuterosomal region, while SPAG5 is enriched in the
1109 deuterosome core. Scale bars: $5\mu\text{m}$ (**d, e**, large view), $1\mu\text{m}$ (**d, e**, high magnification).

1110

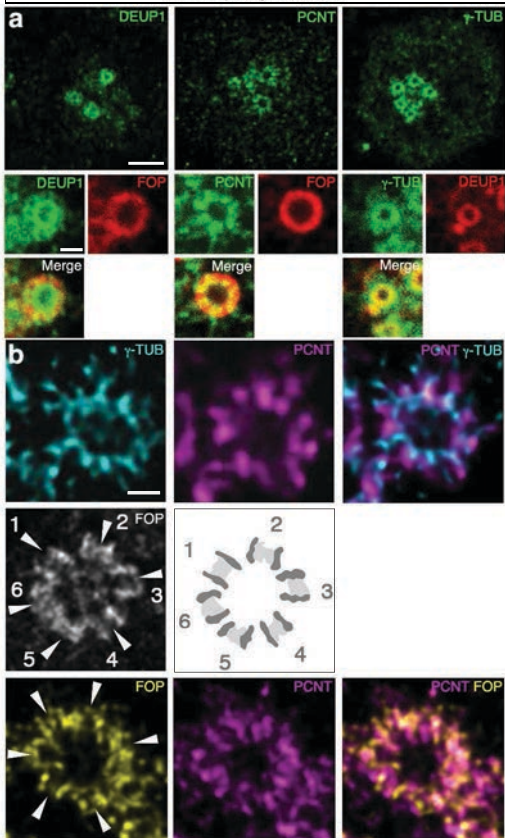
1111 **Figure 7: Separase overexpression rescues multiciliogenesis in absence of Cdc20b.**

1112 **(a-f)** 8-cell *Xenopus* embryos were injected in the presumptive epidermis with *GFP-gpi*
1113 mRNA, *cdc20b* morpholinos, and human *Separase* mRNA, as indicated. Embryos were fixed
1114 at tailbud st25 and immunostained against GFP (injection tracer, green), Acetylated- α -
1115 Tubulin (cilia, white) and γ -Tubulin (BBs, red). White dotted lines indicate the position of
1116 orthogonal projections shown in bottom panels. Red arrowheads point undocked BBs. Left
1117 inset in **(e)** shows zoom on clustered centrioles. **(g)** Bar graph showing the number of
1118 properly ciliated MCCs among injected cells, per field of observation. Bars are standard error

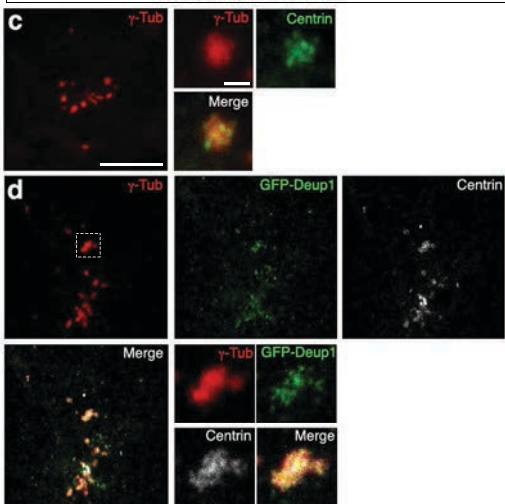
1119 **mean.** Counting was performed on pictures taken at low magnification (20x), in order to score
1120 a large number of cells. Separase overexpression fully rescued multiciliogenesis in *cdc20b*
1121 morphant MCCs. **One way ANOVA and Bonferroni's Multiple Comparisons on two**
1122 **experiments, *** = $p < 0.0001$; ns = $p > 0.05$.** Scale bars: 5 μ m (**a**). (**h**) Model illustrating the
1123 analogy between centriole disengagement in mitotic cells and centriole release from
1124 deuterosomes in post-mitotic MCCs.
1125
1126

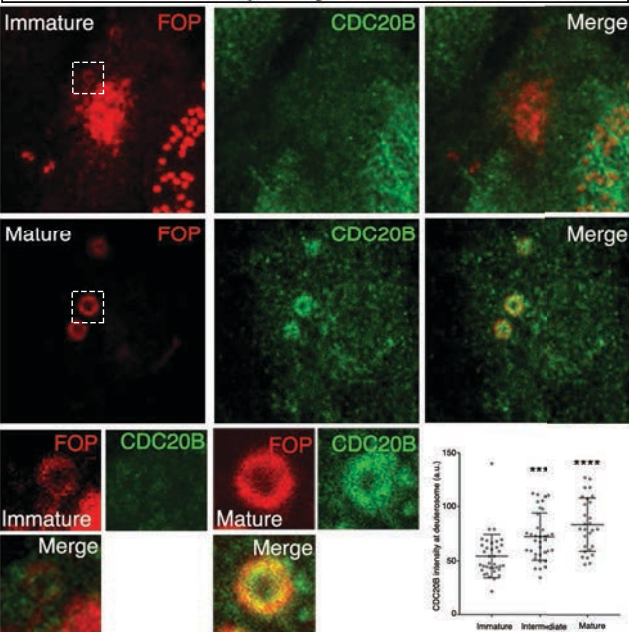
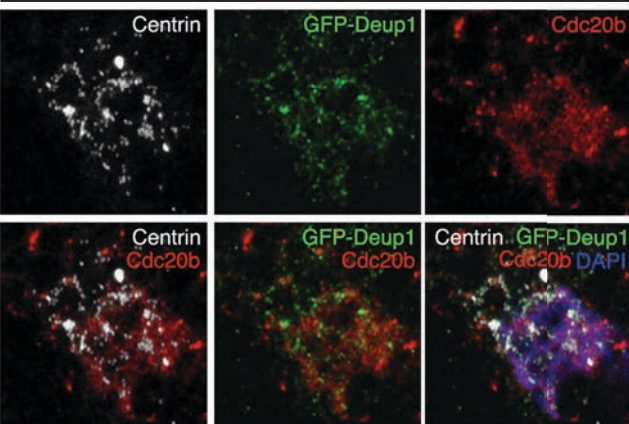


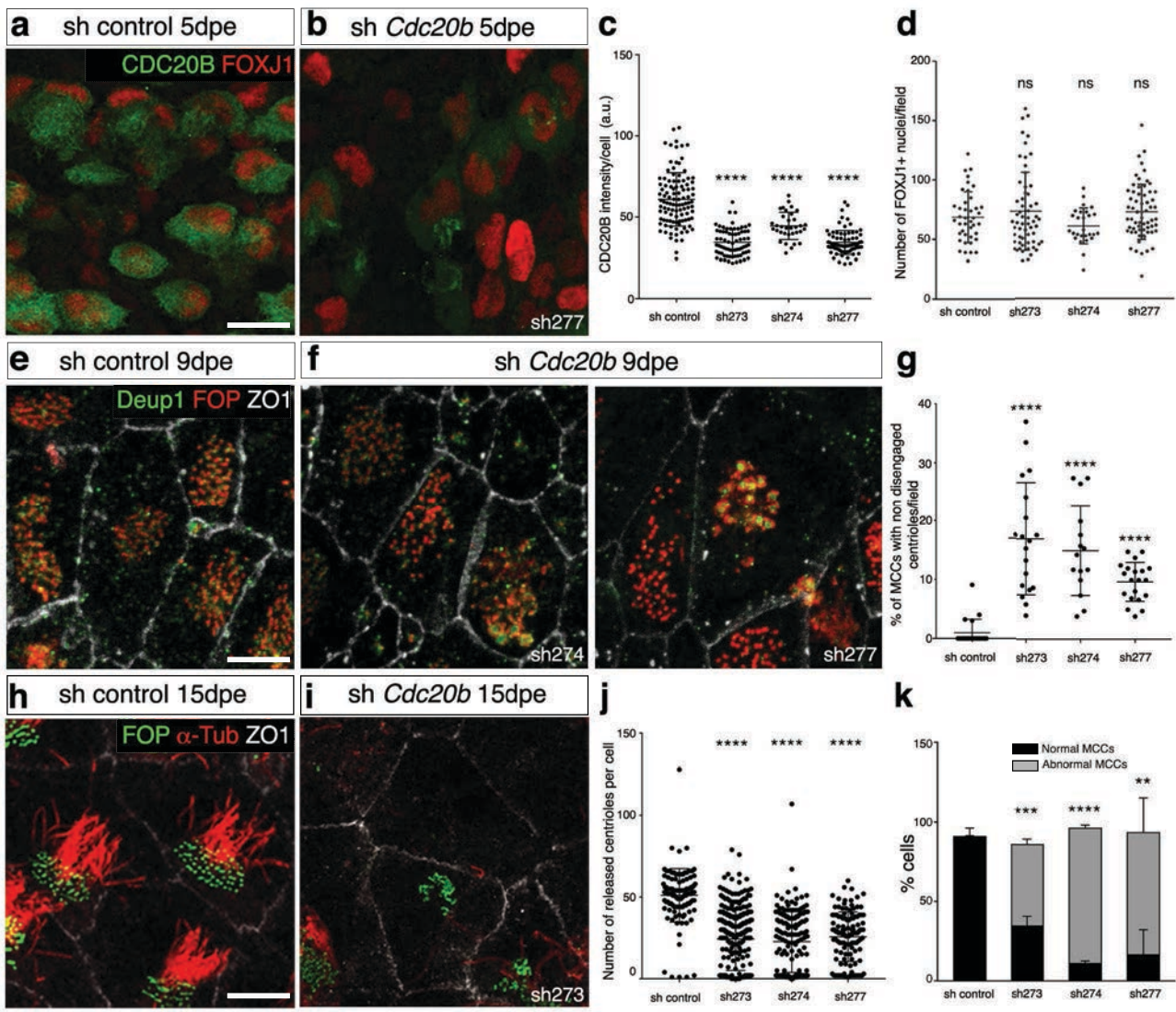
Mouse ependymal MCCs

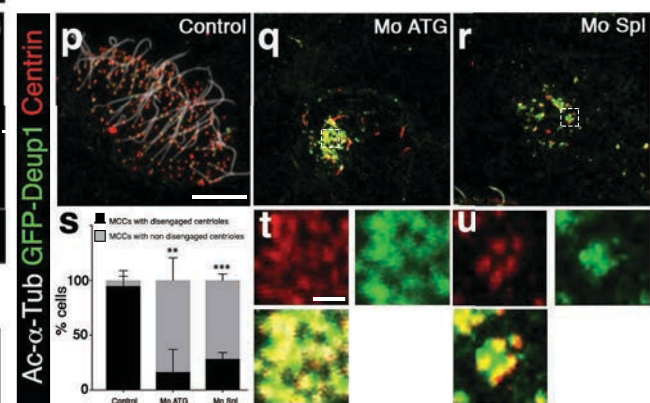
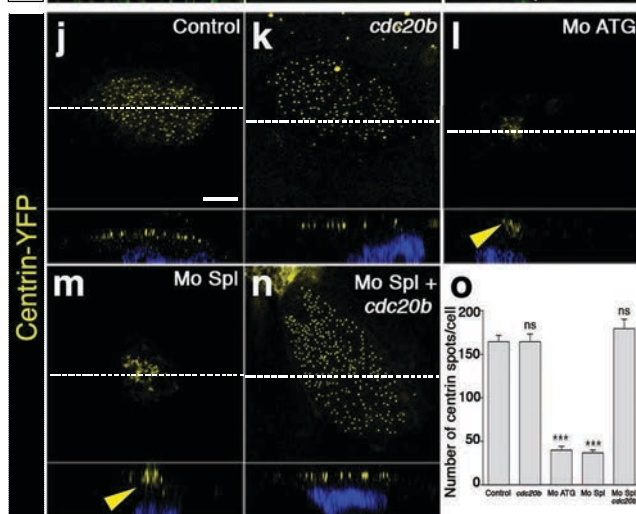
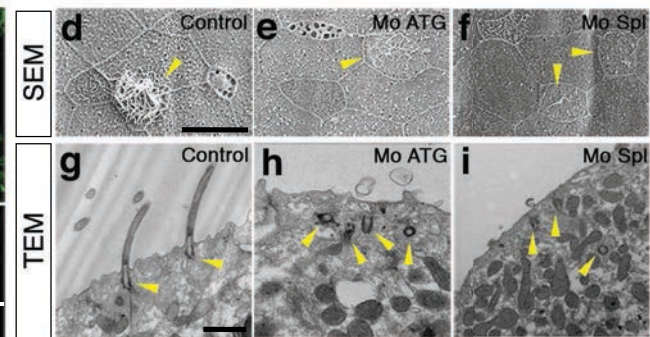
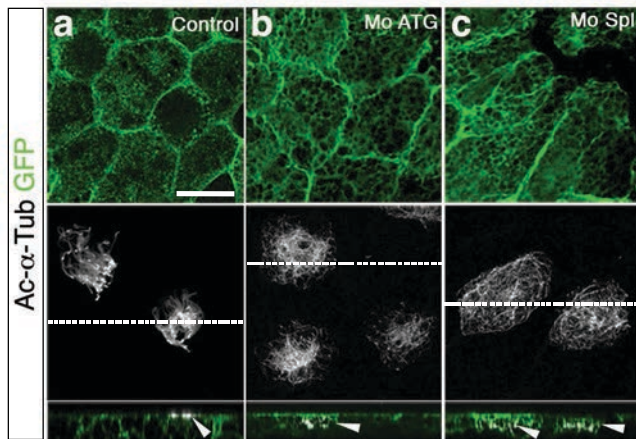


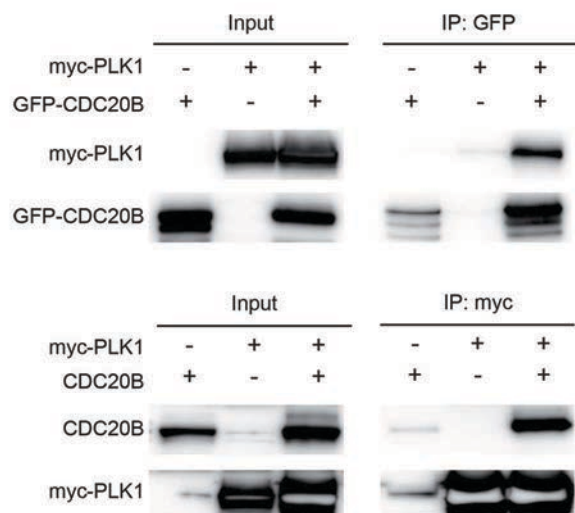
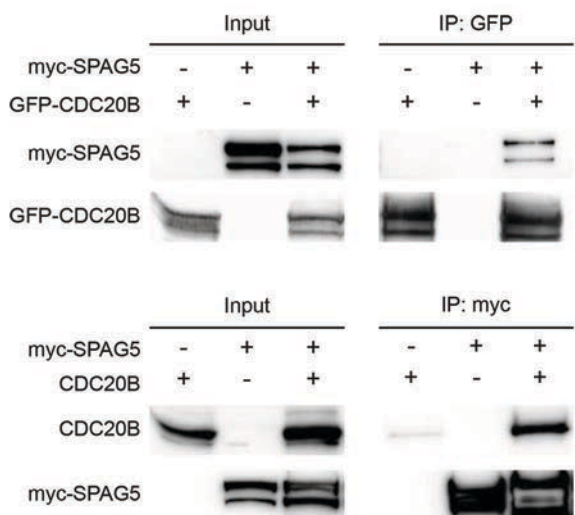
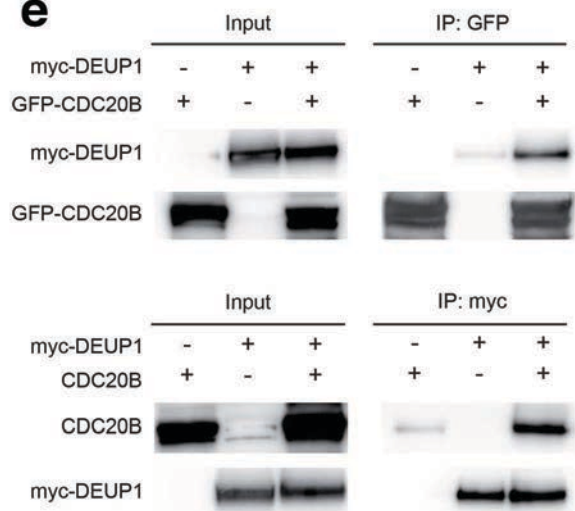
Xenopus epidermis MCCs



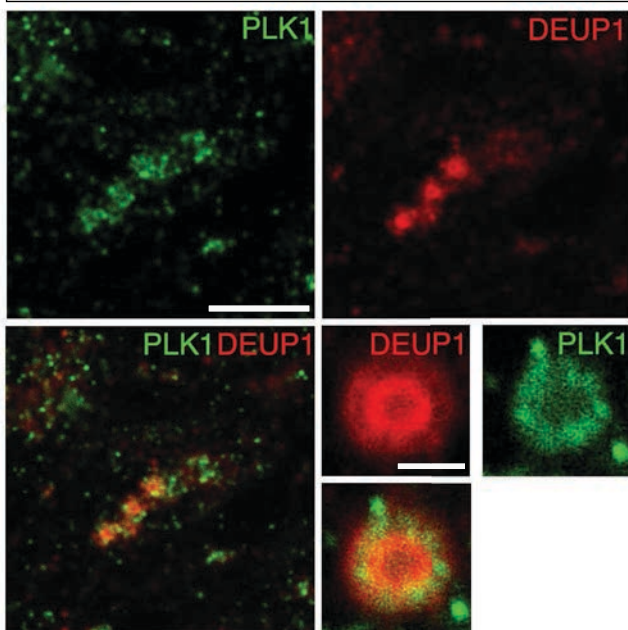
a Mouse tracheal MCCs**b** Mouse ependymal MCCs**c** *Xenopus* epidermis MCCs



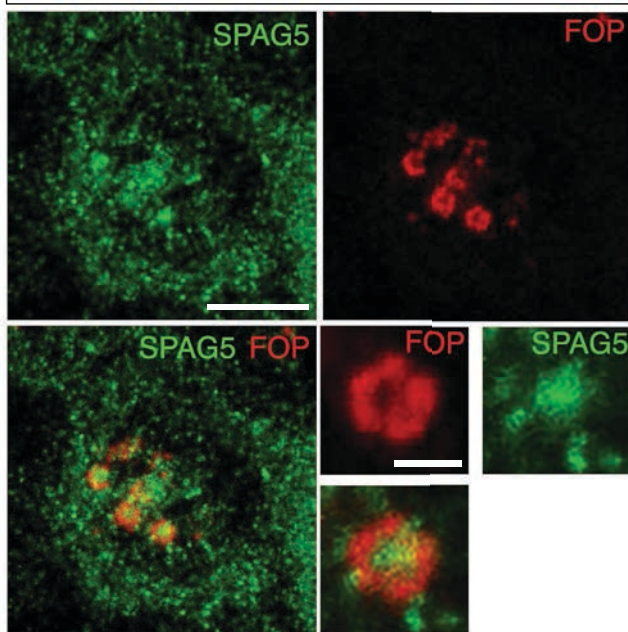


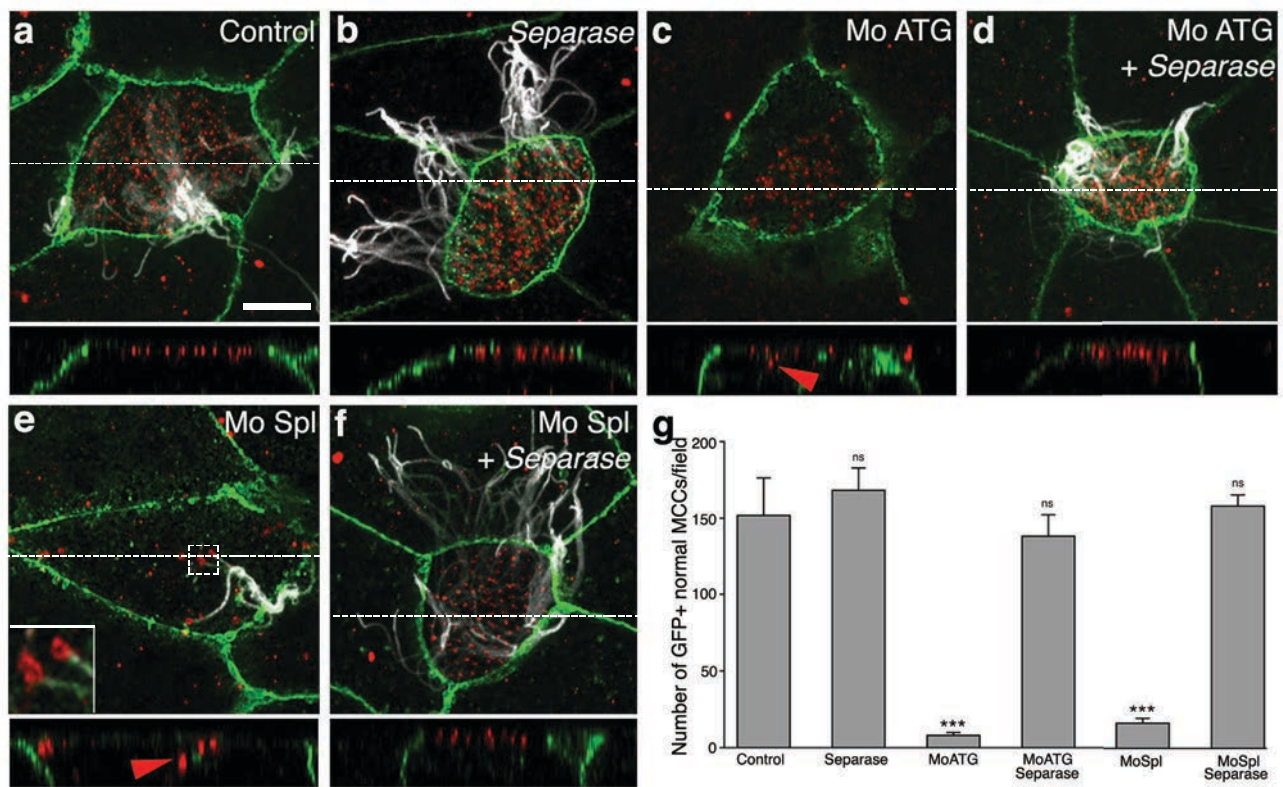
a**c****e****b**

Mouse ependymal MCCs

**d**

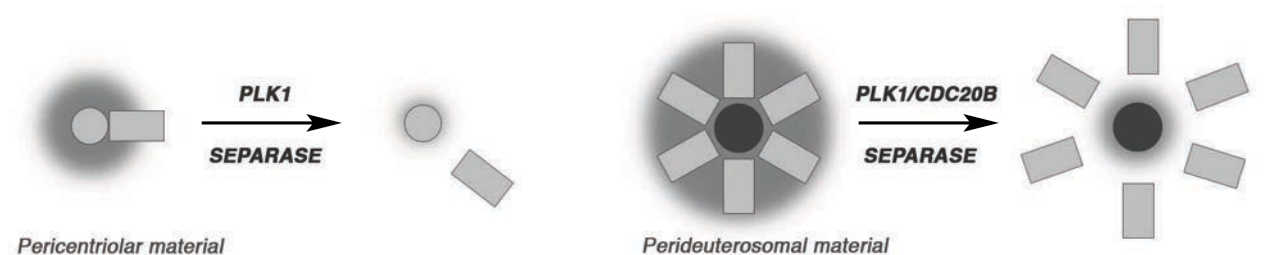
Mouse ependymal MCCs





h Centriole disengagement in mitotic cells

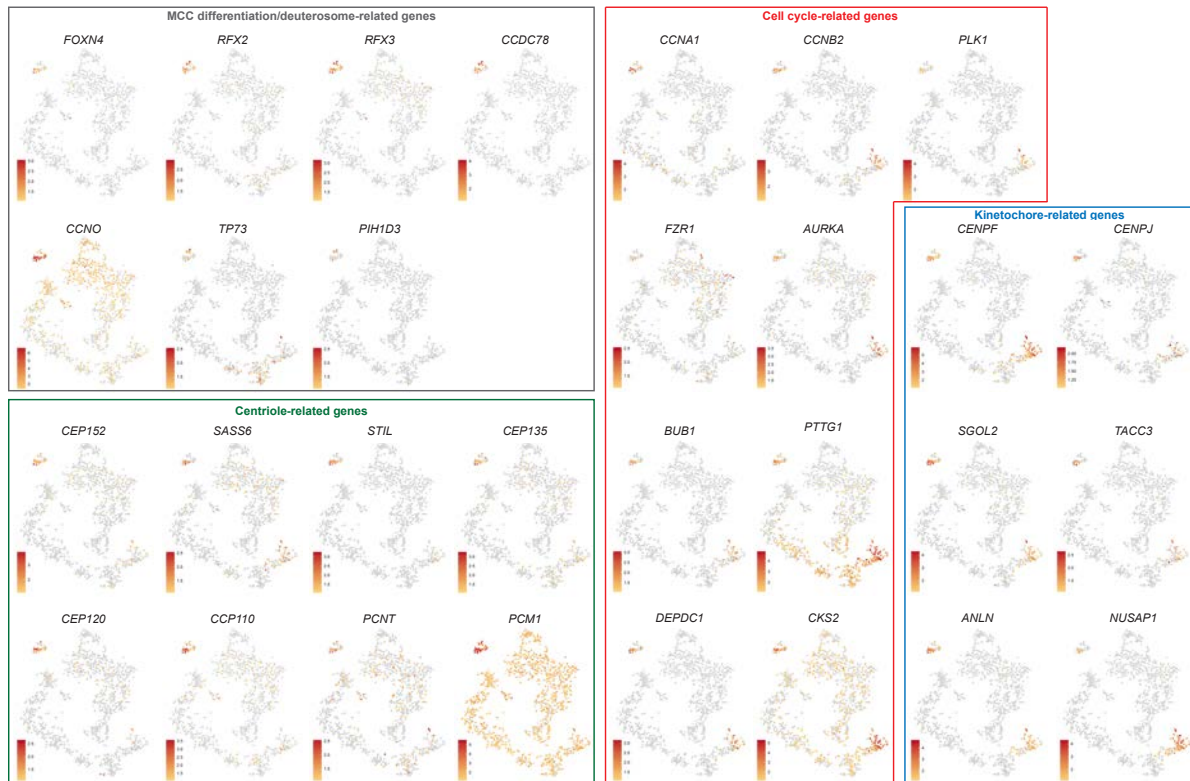
Centriole release from deuterosome in post-mitotic MCCs



Supplementary information

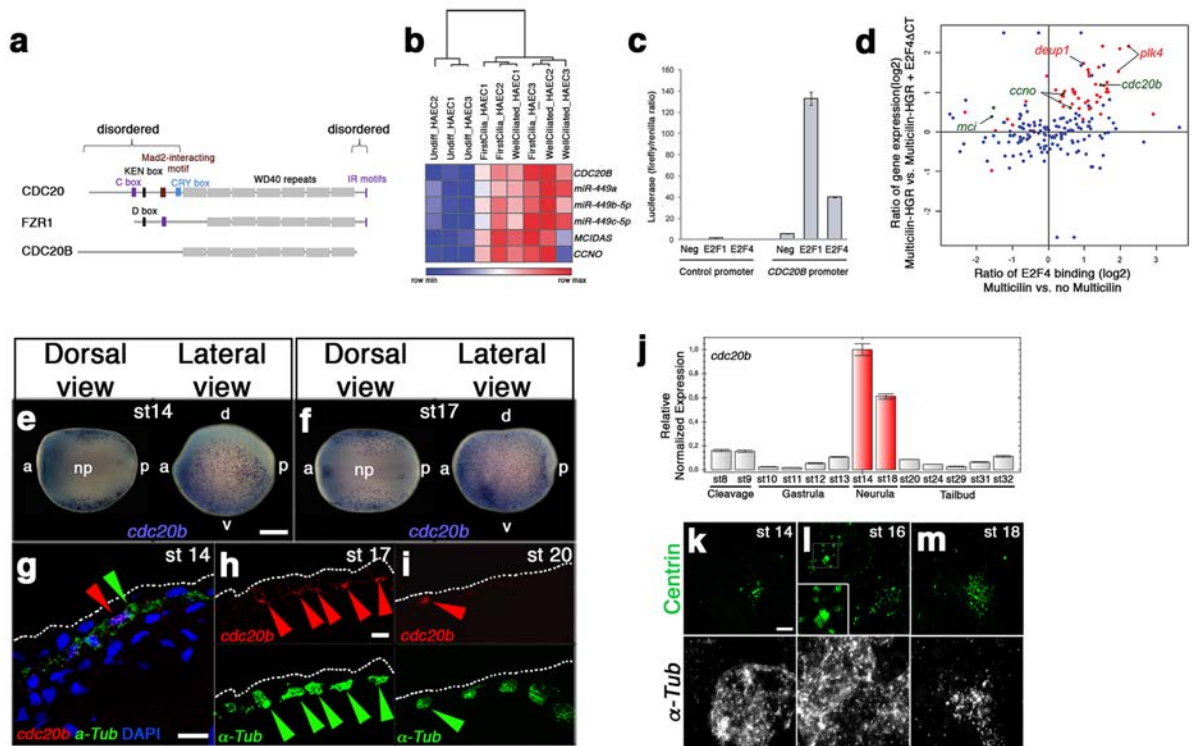
CDC20B is required for deuterosome-mediated centriole production in multiciliated cells

Revinski et al.



Supplementary Figure 1: Single cell RNA-seq analysis of HAECs.

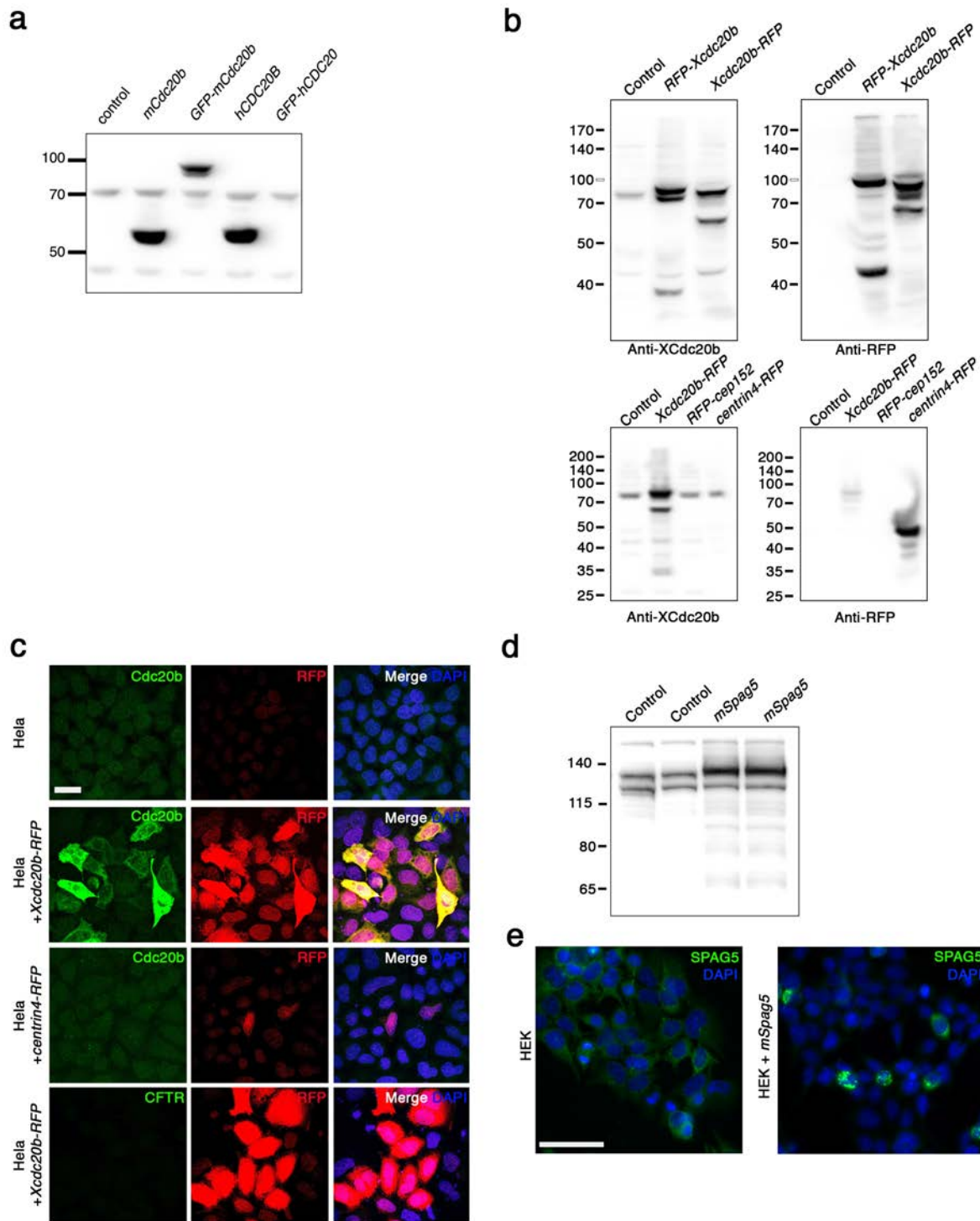
tSNE plots for a selection of genes expressed at the single-cell level, in deuterosomal-stage differentiating HAECs. Genes were grouped into functional categories.



Supplementary Figure 2: Structure, regulation and spatio-temporal expression of *cdc20b*.

(a) Domain composition of CDC20 family members. The C box and IR motifs in CDC20 and FZR1 serve as APC/C binding domains. The KEN box and the Cry box in CDC20, and the D box in FZR1 are involved in their regulation by degradation. The Mad2-interacting motif in CDC20 is important for its regulation by the spindle assembly checkpoint. WD40 repeats are involved in substrate recognition. Note that CDC20B lacks degradation motifs and the APC/C binding domains present in CDC20 and FZR1. **(b)** Heatmap of gene expression measured by RNA-seq or small RNA-seq on 3 independent HAEC differentiation time courses (HAEC1 to HAEC3). Normalized read counts were Log₂-transformed and median-centered by gene. Hierarchical clustering (Euclidian distance) was performed on samples. The scale color bar indicates the minimum and maximum values per row. **(c)** Promoter luciferase reporter assay. Promoter-associated firefly luciferase was normalized to constitutive renilla luciferase. Control and *CDC20B* promoter were co-expressed with a plasmid expressing E2F1 or E2F4, or a negative control. Bars represent the average of 3 independent experiments. Error bars represent

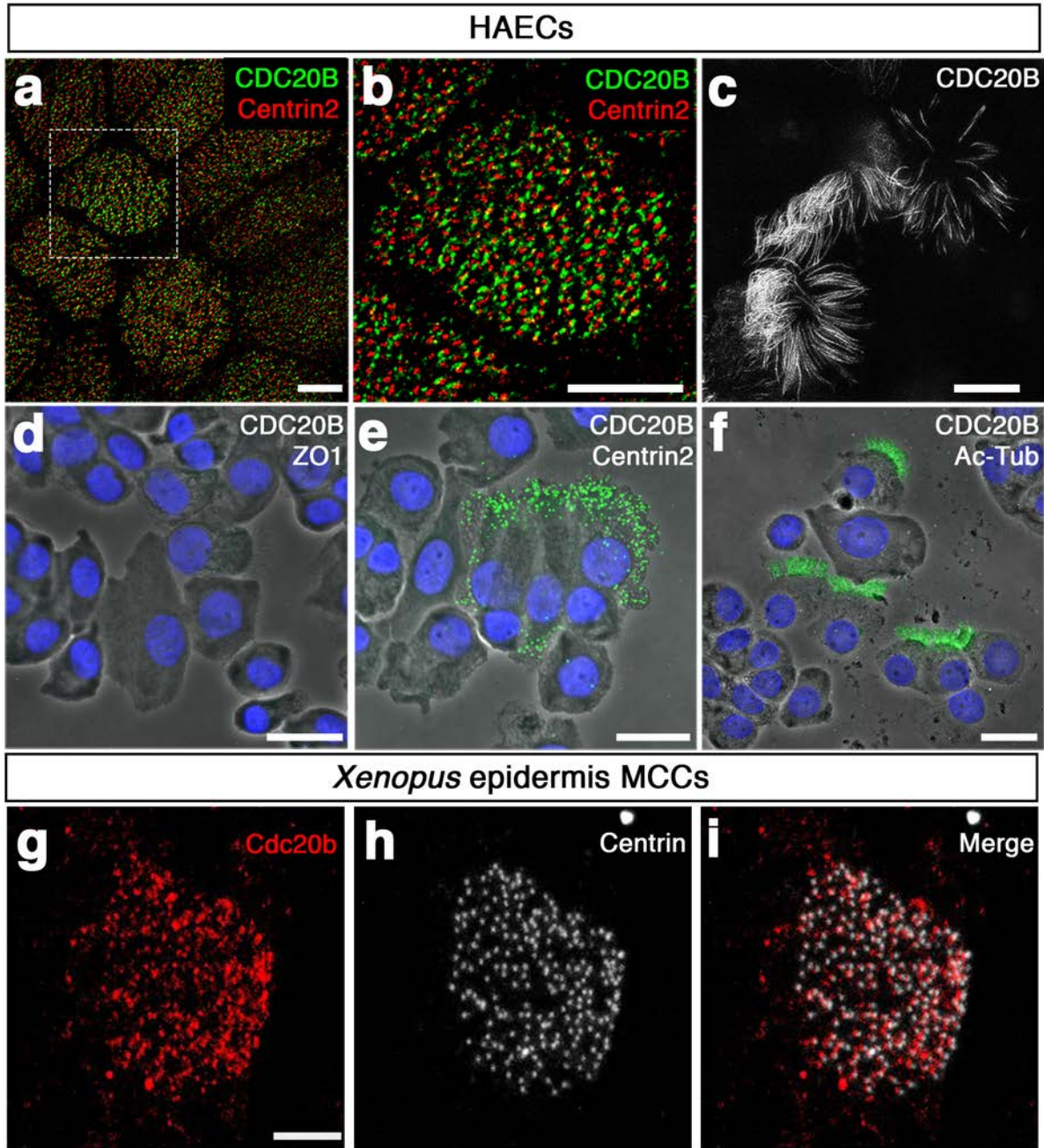
the standard deviation. **(d)** Ratio of gene expression (Multicilin-HGR vs. Multicilin-HGR +E2F4 Δ CT) vs. ratio of E2F4 binding (Multicilin vs. no Multicilin). E2F4 Δ CT prevents the formation of transcriptionally active Multicilin/E2F complexes. Centriole-related genes are highlighted in red. Genes from the multiciliary locus are highlighted in green. The graph was built by mapping and quantifying previously published raw data⁹. **(e,f)** *cdc20b* whole-mount *in situ* hybridization in early *Xenopus laevis* neurula st14 and st17, respectively. *cdc20b* mRNA is expressed in epidermal cells but not in the neural plate (np), as revealed on dorsal views. a: anterior, p: posterior, d: dorsal, v: ventral. **(g-i)** *cdc20b* (red) and α -Tubulin (α -Tub, green) double fluorescent *in situ* hybridization (FISH) on sectioned embryos at st14 **(g)**, st17 **(h)** and st20 **(i)**. Red and green arrows point immature MCCs co-expressing *cdc20b* and α -Tub. Nuclei are revealed by DAPI staining in blue. White dotted lines indicate the surface of the epidermis. Note that the majority of MCCs become negative for *cdc20b* expression at st20. **(j)** RT-qPCR showing the relative expression of *cdc20b* from st8 (mid-blastula transition) until tadpole st32 normalized to *ODC* expression. Red bars indicate the peak of *cdc20b* transcript accumulation between st14 and st18, when centriole amplification occurs. **(k-m)** To reveal the dynamics of centriole multiplication, MCCs were stained by α -Tub FISH and by immunostaining against Centrin. Multiple Centrin-positive foci were detected at st14, marking the onset of centriologensis. Procentriole aggregates, presumably organized around deuterosomes were clearly visualized at st16 (inset). Dispersed multiple centrioles were detected at st18. Scale bars: 250 μ m **(e)**, 20 μ m **(g,h)**, 5 μ m **(k)**.



Supplementary Figure 3: Antibody validations

(a) COS1 cells were transfected with vectors coding for the indicated proteins and immunoblot was performed using Proteintech rabbit antibody raised against human CDC20B. This antibody recognized human and mouse CDC20B but did not cross-react with human CDC20. (b) HeLa cells were transfected with vectors coding for the indicated proteins and immunoblot was

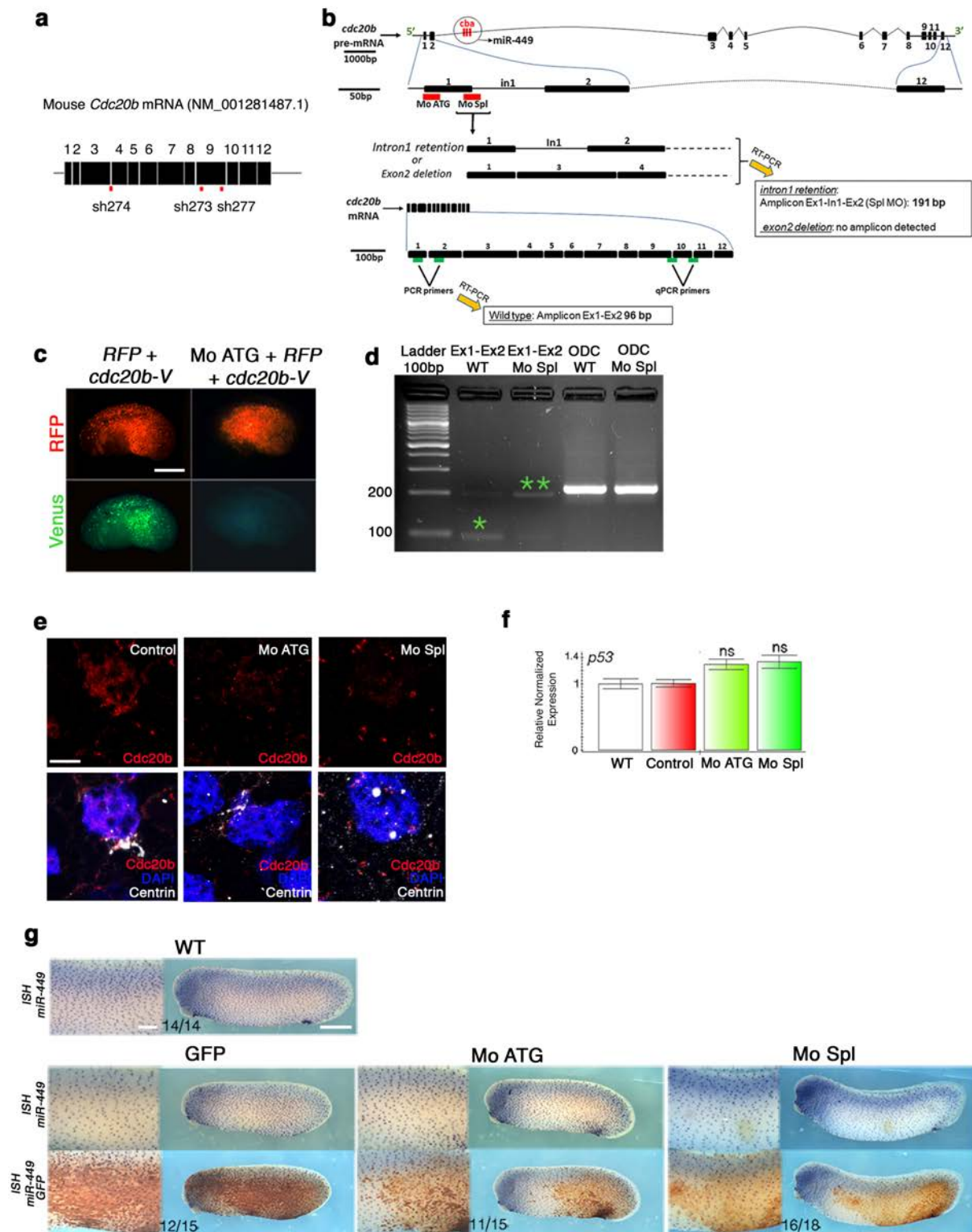
performed using a custom-made rabbit antibody raised against *Xenopus* CDC20B. (c) HeLa cells were transfected with vectors coding for the indicated proteins and immunostainings were performed using the antibodies indicated on the photographs. Note that the antibody directed against *Xenopus* CDC20B did not cross-react with the centriole marker Centrin4. (d) HEK cells were transfected in duplicate with pCMV6-mSpag5, lysed 24 hours later and western blot was performed using proteintech rabbit polyclonal antibody raised against human SPAG5. (e) HEK cells were transfected with pCMV6-mSpag5, fixed with methanol 24 hours later and immunostained using proteintech rabbit polyclonal antibody raised against human SPAG5. This antibody cross-reacted with mouse SPAG5. Scale bars: 20 μ m (c), 50 μ m (e).



Supplementary Figure 4: CDC20B localization in mature MCCs.

(a-f) CDC20B sub-cellular localization in human mature MCCs. (a,b) ALI day 21 HAECs were fixed in methanol, and immunostained against CDC20B and Centrin2. STED super-resolution microscopy revealed the association of CDC20B to BBs. (c) ALI day 21 HAECs were fixed in paraformaldehyde, and immunostained against CDC20B. STED super-resolution microscopy revealed the association of CDC20B with cilia. (d-f) DuoLink Assays on fully

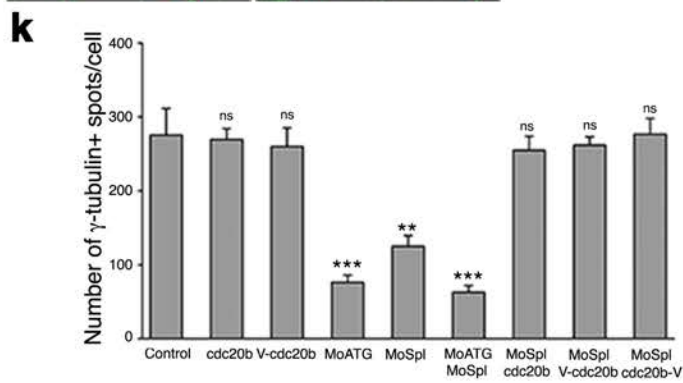
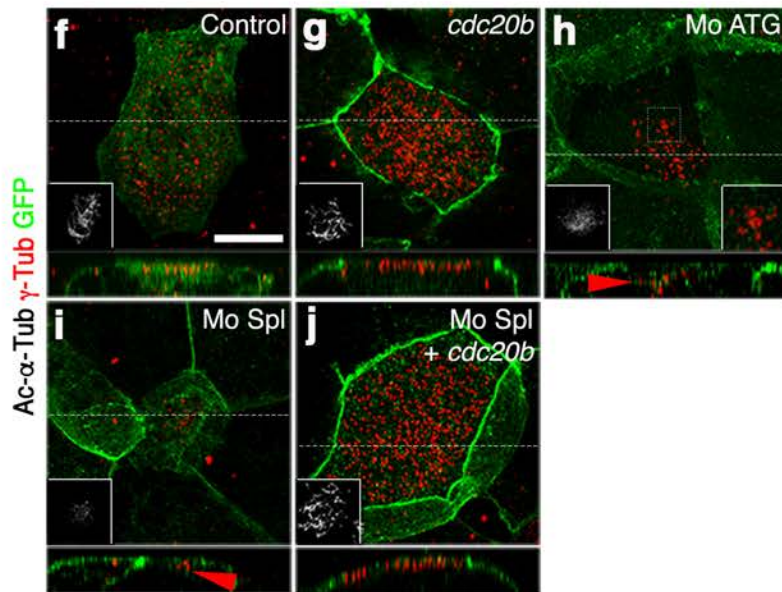
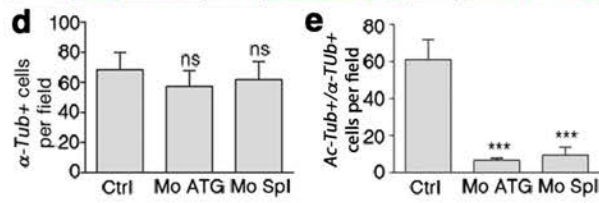
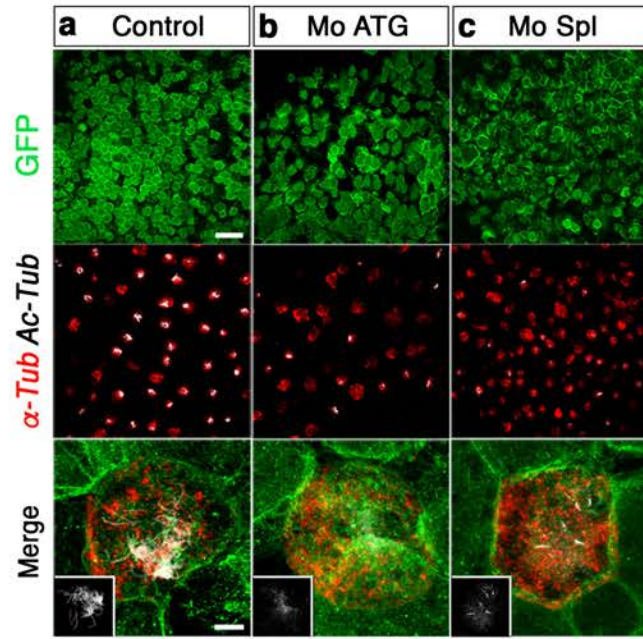
differentiated HAECs after cytopsin. **(d)** Assay with CDC20B and ZO-1 antibodies was used as negative control. **(e)** Assay with CDC20B and Centrin2 (BBs) antibodies. **(f)** Assay with CDC20B and Acetylated- α -Tubulin (cilia) antibodies. Interaction between antibodies separated by less than 40nm generated green fluorescent signal. Nuclei are stained in blue. **(g-i) Cdc20b sub-cellular localization in *Xenopus* mature MCCs.** 4-cell *Xenopus* embryos were injected with *Multicilin-hGR* mRNA, induced with dexamethasone at stage 10.5 to activate Multicilin and immunostained for CDC20B **(g)** and Centrin **(h)** at stage 23. Scale bars: 5 μ m **(a-c)**, 20 μ m **(d-f)**, 5 μ m **(g)**.



Supplementary Figure 5: *cdc20b* knockdown in mouse and *Xenopus*.

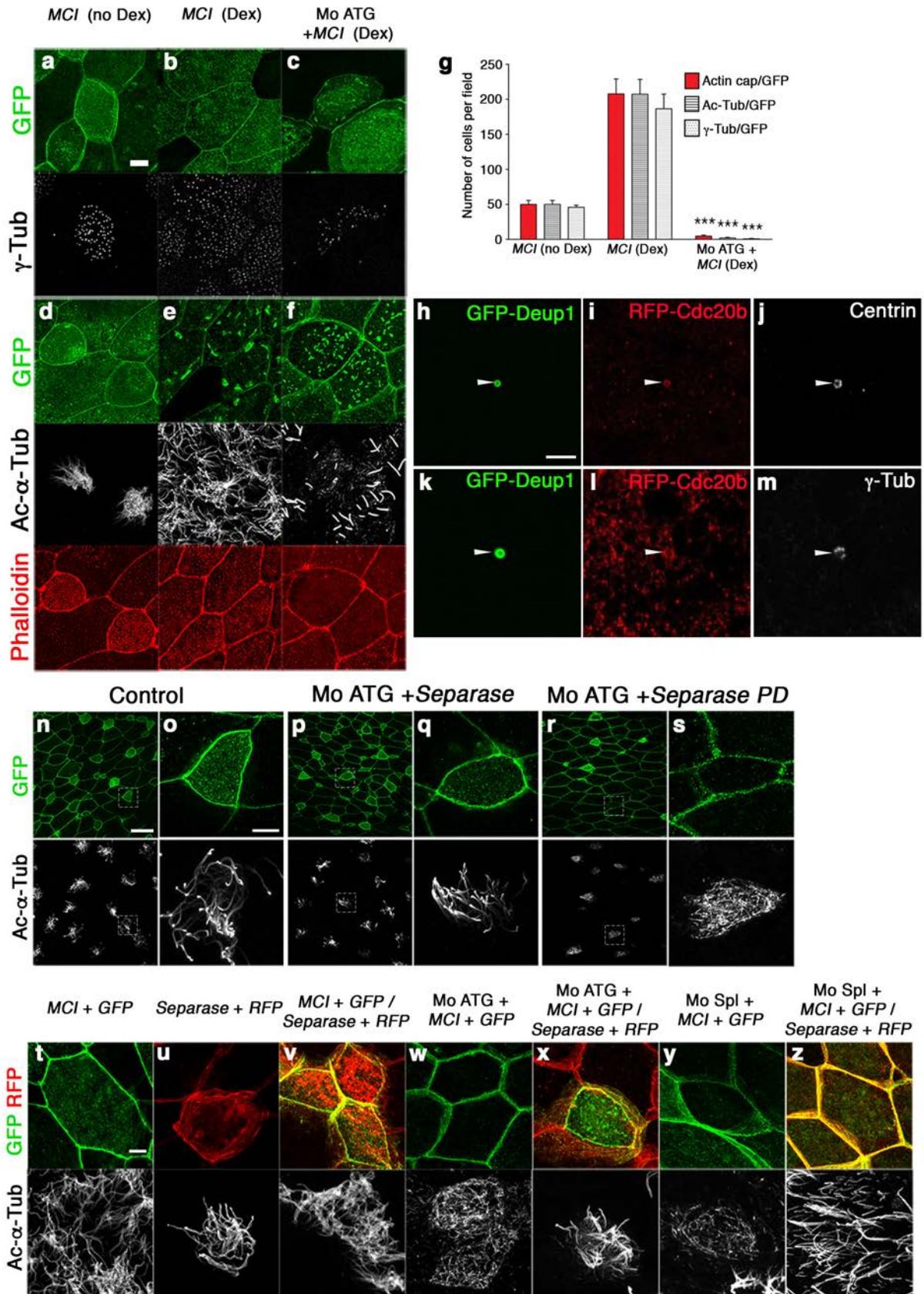
(a) Schematic representation of mouse *Cdc20b* mRNA and position of shRNAs used in this study. Note that sh274 targets the junction between exons 3 and 4, ruling out possible

interference with the production of miR-449 molecules from the *Cdc20b* pre-mRNA. **(b)** Schematic representation of *Xenopus cdc20b* pre-mRNA with introns, exons and miR-449abc relative position and size. Red horizontal bars below exon1 show the position of *cdc20b* Mo ATG and Mo Spl. On the bottom, green horizontal bars indicate RT-PCR and qPCR primer positions. **(c)** The efficiency of Mo ATG was verified through fluorescence extinction of co-injected *cdc20b-Venus*. **(d)** RT-PCR confirmed that Mo Spl caused intron1 retention (amplicon=191bp; double green stars), which is expected to introduce a premature stop codon and to produce a Cdc20b protein lacking 96% of its amino-acids, likely to undergo unfolded protein response-mediated degradation. **(e)** Immunostaining with the anti-*Xenopus* CDC20B antibody confirmed that both Mo ATG and Mo Spl severely down-regulated CDC20B protein expression in st18 MCCs. **(f)** RTqPCR revealed that neither *cdc20b* morpholinos caused significant *p53* transcript up-regulation, a non-specific response sometimes detected in zebrafish embryos subjected to morpholinos. Four independent experiments were carried out to check *p53* expression in morphant conditions. **(g)** miR-449 expression revealed by whole-mount *in situ* hybridization with LNA probes was not perturbed in the presence of either morpholinos. Embryos were photographed before (top) and after (bottom) staining against co-injected GFP-CAAX to be able to detect miR-449 staining. The number of embryos showing normal miR-449 expression over the total number of embryos analyzed is indicated on the photographs. Scale bars: 500 μ m **(c)**, 5 μ m **(e)**, 500 μ m **(g, whole embryo)**, 80 μ m **(g, zoom)**.



Supplementary Figure 6: *cdc20b* knockdown impairs multiciliogenesis in *Xenopus*.

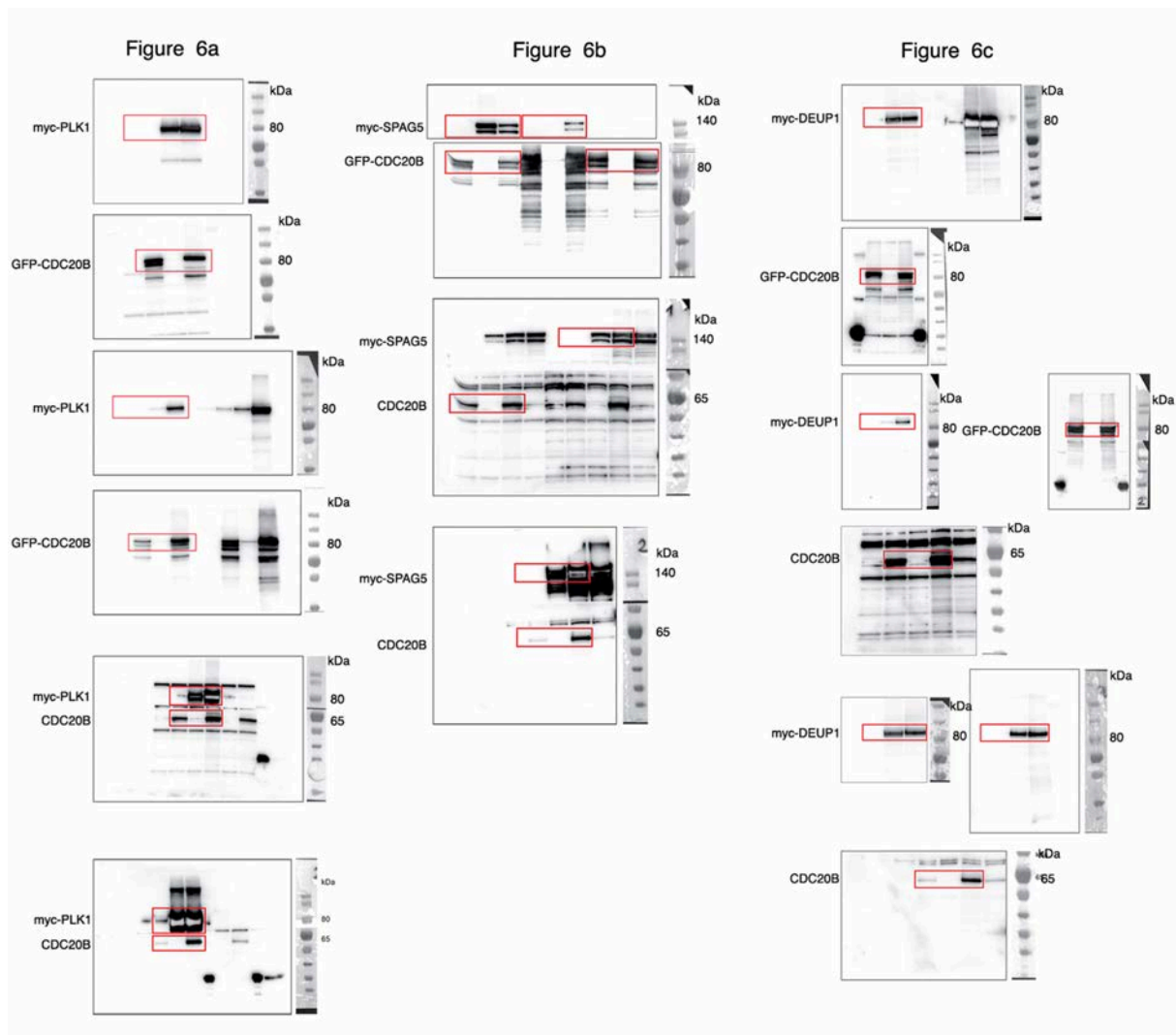
(a-e) 8-cell embryos were injected in presumptive epidermis with *cdc20b* morpholinos and *GFP-CAAX* mRNA (injection tracer) as indicated. Control was provided by *GFP-CAAX* injection alone. Embryos at tailbud st25 were processed for fluorescent staining against GFP (green), Acetylated α -Tubulin (cilia, white) and *α -Tub* mRNA (MCC marker, red). Insets on merged panels show cilia staining. Note that *cdc20b* morphant MCCs maintain expression of fate marker *α -Tub* but poorly grow cilia. (d) Bar graph showing quantification of *α -Tub*/GFP double positive cells per field of observation. (e) Bar graph showing quantification of *α -Tub*/Ac-Tub/GFP triple positive cells per field of observation. 10 fields corresponding to 10 different embryos were analyzed for each condition. (f-k) 8-cell embryos were injected in presumptive epidermis with *cdc20b* morpholinos, *GFP-CAAX* and *cdc20b* mRNAs as indicated, and immunostained at tailbud st25 against GFP (injection tracer, green), γ -tubulin (BBs, red) and Acetylated α -Tubulin (cilia, white, left insets). Right inset in h: zoom on a stalled deuterosomal figure. z-projections made along white dotted lines are shown in bottom panels. Arrowheads point undocked BBs. (k) Bar graph showing the quantification of γ -tubulin spots per MCC. As two individual γ -tubulin spots are detected around each basal body, twice as many spots are usually counted as compared to Centrin (Fig. 5j-o). Note that BB numbers were restored to normal levels in *cdc20b* Spl morphants injected with tagged and untagged versions of *cdc20b*. Scale bars: 50 μ m (a, top), 5 μ m (a, bottom), 5 μ m (f).



Supplementary Figure 7: *cdc20b* knockdown prevents multiciliogenesis induced by Multicilin, and is counteracted by Separase overexpression.

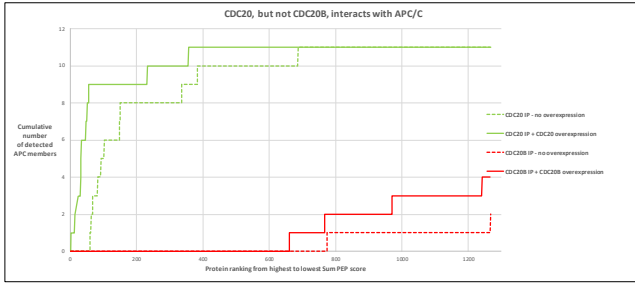
(a-g) *cdc20b* knockdown prevents multiciliogenesis induced by Multicilin. 8-cell embryos were injected in presumptive epidermis with *Multicilin-hGR* mRNA (*MCI*) and *cdc20b* Mo ATG, as indicated. *GFP-GPI* mRNA was co-injected as a tracer. MCI-hGR-injected embryos were induced with dexamethasone at st11. To check the efficiency of MCI induction some embryos were not treated with dexamethasone and served as controls (no DEX). Embryos were fixed at tailbud st25, and were stained against GFP (green) and γ -Tubulin (basal bodies, white)(**a-c**), or against GFP (green), phalloidin (apical actin, red), and Acetylated- α -Tubulin (cilia, white)(**d-f**). Note that *cdc20b* morphant MCI-induced MCCs failed to amplify centrioles, to maintain a proper actin cap, and to grow cilia. (**g**) Bar graph showing the quantification of GFP-positive cells that displayed normal actin, basal body and cilium staining. 5 fields (40x) per condition were analyzed. **(h-m) Deup1 recruits CDC20B in centriole amplification platforms.** 8-cell embryos were injected in presumptive epidermis with *Multicilin-hGR*, *RFP-CDC20B*, and *GFP-Deup1* mRNAs. Multicilin activity was induced with dexamethasone at st11, embryos were fixed at st18 and stained for GFP, RFP, Centrin (centrioles) or γ -Tubulin (deuterosome). White arrowheads point a centriole amplification platform positive for GFP-Deup1, which incorporates RFP-CDC20B, consistent with their capacity to form a complex (Fig. 6c). **(n-z) Wild-type but not protease-dead Separase rescues multiciliogenesis in MCCs deficient for Cdc20b.** **(n-s)** 8-cell embryos were injected in presumptive epidermis with *GFP-GPI* mRNA, human *Separase* mRNA, and *cdc20b* Mo ATG, as indicated. Immunofluorescence against GFP (injection tracer, green), and Acetylated- α -Tubulin (cilia, white) was performed at tailbud st25. Cells in dotted squares were blown up for better visualization. Note that multiciliogenesis was rescued in *cdc20b* morphant MCCs by wild-type **(p,q)** but not protease-dead Separase **(r,s)**. **(t-z)** 4-cell embryos were injected in one ventral blastomere (presumptive epidermis) with *MCI-hGR* and *GFP-GPI* mRNAs, in the presence or not of *cdc20b* morpholinos, as indicated. Next, at 16-cell stage, half of those embryos were

injected with human *Separase* and RFP mRNAs in one ventral-animal blastomere. This setup was designed to avoid co-injection of *cdc20b* morpholinos with *Separase* mRNA, ruling out non-specific interference *in vitro* between these reagents. MCI-hGR-injected embryos were induced with dexamethasone at st11. All embryos were fixed at tailbud st25 and stained for GFP (*cdc20b* Mo tracer, green), RFP (*Separase* tracer, red) and Acetylated- α -Tubulin (cilia, white). Note that multiciliogenesis failed in MCI-induced *cdc20b* morphant MCCs (**w,y**). The presence of *Separase* rescued multiciliogenesis in MCI-induced *cdc20b* morphant MCCs (**x,z**). Scale bars: 5 μ m (**a, h, o, t**), 20 μ m (**n**).



Supplementary Figure 8: Uncropped Western blots.

Red boxes mark the parts of the Western blot images that are shown in the indicated parts of Figure 6.



IP: CDC20 - no overexpression												
Protein FDR Confidence	Accession	Symbol	Description	Sum PEP Score/Coverage	#Peptides	#PSMs	#Unique Peptides	MW (kDa)	empAI	Score Sequent HT	global rank	APC rank
High	ORU02	CDC20	Cell division c	109.78	27	48	27	68.79	6.80	88.85	60	1,00
High	Q12834	CDC20	Cell division c	104.51	49.70	16	16	54.69	10.94	158.30	63	2,00
High	OR1144	ANAPC1	Anaphase pro	101.92	21.06	12	12	216.16	1.30	38.70	68	1,00
High	ORU144	ANAPC5	Anaphase pro	91.89	42.38	23	23	85.02	3.19	83.00	82	4,00
High	ORU133.AQAD248B13	ANAPC7	Anaphase pro	85.18	45.58	21	21	66.61	6.13	63.05	92	5,00
High	AQAD248DZ2.Q13042	CDC16	CDC16 cell div	79.32	43.55	21	21	71.61	4.37	48.14	102	6,00
High	P30260	CDC27	Cell division c	63.63	26.33	16	16	91.61	2.00	41.46	148	7,00
High	GEF36	CDC27	Cell division c	63.28	26.25	16	16	91.68	2.00	41.49	150	8,00
High	ORU16	ANAPC2	Anaphase pro	37.09	22.75	13	13	93.77	0.93	15.24	336	9,00
High	ORU145	ANAPC4	Anaphase pro	31.68	15.34	13	13	92.06	0.81	7.07	383	10,00
High	ORU113	ANAPC10	Anaphase pro	15.61	11.89	5	5	71.24	1.85	11.56	686	11,00

IP: CDC20 + CDC20 overexpression												
Protein FDR Confidence	Accession	Symbol	Description	Sum PEP Score/Coverage	#Peptides	#PSMs	#Unique Peptides	MW (kDa)	empAI	Score Sequent HT	global rank	APC rank
High	OR1144	ANAPC1	Anaphase pro	710.46	59.57	81	81	216.36	28.94	640.59	2	1
High	ORU144	ANAPC5	Anaphase pro	483.89	65.73	50	50	85.02	142.07	635.28	13	2
High	ORU145	ANAPC4	Anaphase pro	371.59	59.53	43	43	92.06	34.74	384.67	24	3
High	Q12834	CDC20	Cell division c	332.93	69.54	28	28	54.69	202.09	1712.61	28	3
High	P30260	CDC27	Cell division c	305.64	60.56	34	34	91.61	20.92	435.97	31	4
High	GEF36	CDC27	Cell division c	306.44	60.51	34	34	91.68	20.92	426.79	32	5
High	ORU16	ANAPC2	Anaphase pro	301.10	54.50	45	45	93.77	17.12	293.57	33	6
High	AQAD248DZ2.Q13042	CDC16	CDC16 cell div	233.91	55.00	29	29	71.61	22.90	226.42	47	7
High	ORU162	CDC15	Cell division c	244.48	54.77	33	33	68.79	27.60	262.71	51	8
High	ORU133.AQAD248B13	ANAPC7	Anaphase pro	236.24	64.61	32	32	66.61	37.75	239.65	56	9
High	ORU113	ANAPC10	Anaphase pro	86.65	76.22	11	11	71.24	27.48	96.76	252	10
High	B3.B6	CDC27	Cell division c	63.60	63.09	7	7	25.91	5.81	75.14	357	11

IP: CDC20B - no overexpression												
Protein FDR Confidence	Accession	Symbol	Description	Sum PEP Score/Coverage	#Peptides	#PSMs	#Unique Peptides	MW (kDa)	empAI	Score Sequent HT	global rank	APC rank
High	ORU145	ANAPC4	Anaphase pro	7.09	3.47	1	1	92.06	0.05	0.13	774	1
High	AQAD248DZ2.Q13042	CDC16	CDC16 cell div	2.31	4.68	1	1	71.61	0.06	0.00	1266	1

IP: CDC20B + CDC20B overexpression												
Protein FDR Confidence	Accession	Symbol	Description	Sum PEP Score/Coverage	#Peptides	#PSMs	#Unique Peptides	MW (kDa)	empAI	Score Sequent HT	global rank	APC rank
High	OR1144	CDC20B	Cell division c	215.12	60.89	26	26	57.30	41.99	546.93	7	0
High	AQAD248DZ2.Q13042	CDC16	CDC16 cell div	11.98	12.90	5	5	68.79	0.17	0.00	661	1
High	P30260	CDC27	Cell division c	9.77	5.85	3	3	71.61	0.21	3.53	768	2
High	ORU133.AQAD248B13	ANAPC7	Anaphase pro	6.89	1.64	3	3	91.61	0.17	3.63	871	3
High	ORU113	ANAPC10	Anaphase pro	4.21	6.18	2	2	66.61	0.15	0.00	1242	4

Protein ranking from highest to lowest Sum PEP score	Cumulative number of detected APC members			
	CDC20 IP - no overexpression	CDC20 IP + CDC20 overexpression	CDC20B IP - no overexpression	CDC20B IP + CDC20B overexpression
1	0	0	0	0
2	0	1	0	0
3	0	1	0	0
4	0	1	0	0
5	0	2	0	0
6	0	2	0	0
7	0	3	0	0
8	0	3	0	0
9	0	3	0	0
10	0	3	0	0
11	0	4	0	0
12	0	4	0	0
13	0	4	0	0
14	0	5	0	0
15	0	5	0	0
16	0	5	0	0
17	0	6	0	0
18	0	6	0	0
19	0	6	0	0
20	0	7	0	0
21	0	7	0	0
22	0	7	0	0
23	0	7	0	0
24	0	7	0	0
25	0	7	0	0
26	0	8	0	0
27	0	8	0	0
28	0	8	0	0
29	0	8	0	0
30	0	8	0	0
31	0	9	0	0
32	0	9	0	0
33	0	9	0	0
34	0	9	0	0
35	0	9	0	0
36	0	9	0	0
37	0	9	0	0
38	0	9	0	0
39	0	9	0	0
40	0	9	0	0
41	0	9	0	0
42	0	9	0	0
43	0	9	0	0
44	0	9	0	0
45	0	9	0	0
46	0	9	0	0
47	0	9	0	0
48	0	9	0	0
49	0	9	0	0
50	0	9	0	0
51	0	9	0	0
52	0	9	0	0
53	0	9	0	0
54	0	9	0	0
55	0	9	0	0
56	0	9	0	0
57	0	9	0	0
58	0	9	0	0
59	0	9	0	0
60	0	9	0	0
61	0	9	0	0
62	0	9	0	0
63	0	9	0	0
64	0	9	0	0
65	0	9	0	0
66	0	9	0	0
67	0	9	0	0
68	0	9	0	0
69	0	9	0	0
70	0	9	0	0
71	0	9	0	0
72	0	9	0	0
73	0	9	0	0
74	0	9	0	0
75	0	9	0	0
76	0	9	0	0
77	0	9	0	0
78	0	9	0	0
79	0	9	0	0
80	0	9	0	0
81	0	9	0	0
82	0	9	0	0
83	0	9	0	0
84	0	9	0	0
85	0	9	0	0
86	0	9	0	0
87	0	9	0	0
88	0	9	0	0
89	0	9	0	0
90	0	9	0	0
91	0	9	0	0
92	0	9	0	0
93	0	9	0	0
94	0	9	0	0
95	0	9	0	0
96	0	9	0	0
97	0	9	0	0
98	0	9	0	0
99	0	9	0	0
100	0	9	0	0

Supplementary Table 2: CDC20, but not CDC20B, interacts with APC/C.